

# Functional approach to the error control in adaptive IgA schemes for elliptic boundary value problems

S. Matculevich\*

May 28, 2018

## Abstract

This work presents a numerical study of *functional type* a posteriori error estimates for *IgA approximation schemes* in the context of elliptic boundary-value problems. Along with the detailed discussion of the most crucial properties of such estimates, we present the algorithm of a reliable solution approximation together with the scheme of an efficient a posteriori error bound generation. In this approach, we take advantage of B-(THB-) spline's high smoothness for the auxiliary vector function reconstruction, which, at the same time, allows to use much coarser meshes and decrease the number of unknowns substantially. The most representative numerical results, obtained during a systematic testing of error estimates, are presented in the second part of the paper. The efficiency of the obtained error bounds is analysed from both the error estimation (indication) and the computational expenses points of view. Several examples illustrate that functional error estimates (alternatively referred to as the *majorants* and *minorants* of deviation from an exact solution) perform a much sharper error control than, for instance, residual-based error estimates. Simultaneously, assembling and solving routines for an auxiliary variables reconstruction, which generate the majorant (or minorant) of an error, can be executed several times faster than the routines for a primal unknown.

## 1 Introduction

The investigation of effective adaptive refinement procedures has recently become an active area of research in the context of fast and efficient solvers for isogeometric analysis (IgA) [24, 25]. The adaptivity scheme is naturally linked with reliable and quantitatively efficient a posteriori error estimation tools. The latter ones are expected to identify the parts of a considered computational domain with relatively high discretisation errors and provide a fully automated refinement strategy in order to reach desired accuracy levels for an approximate solution.

Due to a tensor-product setting of IgA splines, mesh refinement has global effects, which include a large percentage of superfluous control points in data analysis, unwanted ripples on the surface, etc. These issues produce certain challenges at the design stage as well as complications in handling big amounts of data, and, therefore, naturally trigger the development of local refinement strategies for IgA. At the moment, four different IgA approaches for adaptive mesh refinement are known, i.e., T-splines, hierarchical splines, PHT-splines, and LR splines.

The localised splines of the first type, *T-splines*, were introduced in [66, 65] and analysed in [1, 4, 63, 64]. They are based on the T-junctions that allow eliminating redundant control points from NURBS model. The thorough study confirmed that this approach generates an efficient local refinement algorithm for *analysis-suitable* T-splines [36] and avoids the excessive propagation of control points. In [3, 9], it was proposed to characterise such splines as dual-compatible T-splines, and in [43] a refinement strategy with linear complexity was described for the bivariate case.

The alternative approach that implies the local control of refinement is based on *hierarchical B-splines* (HB-splines), such that a selected refinement region basis functions are replaced with the finer ones of the same type. The procedure of designing a basis for the hierarchical spline space was suggested in [17, 29, 23] and extended in [70, 16, 62]. Such construction guarantees the linear independence of the basis and provides nested approximation spaces. However, since the partition of unity is not preserved for these splines, *truncated hierarchical B-splines* (THB-splines) have been developed (see [21]). In addition to good stability and approximation properties inherited from HB-splines [19, 67], THB-splines form a convex partition of unity. Therefore, they are

---

\*RICAM Linz, Johann Radon Institute, AT-4040 Linz, svetlana.matculevich@ricam.oeaw.ac.at

suitable for the application in CAD. Various usage of THB-spline for arbitrary topologies can be found, e.g., in [72, 76, 77].

The locally defined splines of the third type, namely, *polynomial splines over hierarchical T-meshes*, are constructed for the entire space of piecewise polynomials with given smoothness on the subdivision of considered domain. The corresponding application can be found in [46, 71]. However, in this case, one must assume the reduced regularity of basis [11] or fulfil a certain constraint on admissible mesh configuration [74]. In [47], the adaptive procedure is based on the recovery-based error estimator, in which discontinuous enrichment functions are added to the IgA approximation.

Finally, *locally refined splines* (LR-splines) rely on the idea of splitting basis functions. This technique achieves localisation but creates difficulties with linear independence [13], which has been studied in [6, 7]. The application of such type of splines has been thoroughly investigated in [13]. In [26], one can find the summary of a detailed comparison of (T)HB-splines and LR splines with respect to sparsity and condition numbers. The study concludes that even though LR splines have smaller support than THB-splines, the numerical experiments did not reveal any significant advantages of the first ones with respect to the sparsity patterns or condition numbers of mass and stiffness matrices.

The refinement tools of IgA mentioned above were combined with various a posteriori error estimation techniques. For instance, the a posteriori error estimates based on hierarchical splines were investigated in [14, 70]. In [27, 71, 8, 30], the authors used the residual-based a posteriori error estimates and their modifications in order to construct mesh refinement algorithms. The latter ones, in particular, require the computation of constants related to the Clement-type interpolation operators, which are mesh-dependent and often difficult to compute for general element shapes. Moreover, these constants must be re-evaluated every time a new mesh is generated. The goal-oriented error estimators, which are rather naturally adapted to practical applications, have lately been introduced for IgA approximations and can be found in [69, 10, 31, 32].

In the current work, the terms *error estimate* and *error indicator* distinguish from each other. The first one is considered as the total upper (or lower) bound of true energy error. These are very important characteristics related to the approximate solution since they can be used to judge whether obtained data are reliable or not. In order to locate the areas of the discretised domain that have the highest error in the approximation, a quantitatively sharp *error indicator* is required. The methods of a posteriori error estimation listed above are rather error indicators in this terminology and indeed were successfully used for mimicking the approximation error distribution. However, their use in the error control, i.e., a reliable estimation of the accuracy of obtained data, is rather heuristic in nature.

Below we investigate a different *functional* method providing fully guaranteed error estimates, the upper (and lower) bounds of the exact error in the various weighted norms equivalent to the global energy norm. These estimates include only global constants (independent of the mesh characteristic  $h$ ) and are valid for any approximation from admissible functional space. One of the most advantageous properties of functional error estimates is their independence of the numerical method used for calculating approximate solutions. The strongest assumption about approximations is that they are conforming in the sense that they belong to a certain natural Sobolev space suited for the problem. It is important to emphasise that this is still a rather weak assumption and that no further restrictions, such as Galerkin orthogonality, are needed.

Functional error estimates were initially introduced in [59, 60] and later applied to different mathematical models summarised in monographs [45, 52, 37]. They provide guaranteed, sharp, and fully computable upper and lower bounds of errors. A pioneering study on the combination of functional type error estimates with the IgA approximations generated by tensor-product splines is presented in [28] for elliptic boundary value problems (BVP). The extensive numerical tests presented in this work confirmed that majorant produces not only good upper bounds of the error but also a quantitatively sharp error indicator. Moreover, the authors suggest the heuristic algorithm that allows using the smoothness of B-splines for a rather efficient calculation of true error upper bound.

The current work further extends the ideas used in [28] for B-splines (NURBS) and combines the functional approach to the error control with THB-splines. Moreover, our focus is concentrated not only on the qualitative and quantitative performance of error estimates but also on the required computation time for their reconstruction. The systematic analysis of majorant's numerical properties is based on a collection of extensive tests performed on the problems of different complexity. For the error control implemented with the help of tensor-structured B-splines (NURBS) and THB-splines, we manage to obtain an impressive speed-up in majorant reconstruction by exploiting high smoothness of B-splines to our advantage. However, for the problems with sharp local changes or various singularities in the solution, the THB-splines implementation in G+Smo restricts the performance speed-up when it comes to solving the optimal system for the error majorant as well as for its element-wise evaluation. We restrict this study only to the domains modelled by a single patch,

which provides at least  $C^1$ -continuity of the approximate solutions inside the patch. However, the application of studied majorants can be extended to a multi-patch domain, since the error estimates for stationary problems are flexible enough to handle fully non-conforming approximations (this issue has been in details addressed in [35, 68, 61]).

The error control for the problems defined on domains of complicated shapes induces another issue related to the estimation of Friedrichs' constant used by functional error estimates not only as the weight but also as the geometrical characteristics of the considered problem. When such domains are concerned, one can perform their decomposition into a collection of non-overlapping convex sub-domains, such that the global constant can be replaced by constants in local embedding inequalities (Poincaré and Poincaré-type inequalities [50, 51]). The reliable estimates of these local constants can be found in [48, 2, 44, 42]. The derivation of functional error estimates exploiting these ideas is discussed in [52, 54] for the elliptic BVP and in [40, 39, 41] for the parabolic initial boundary value problem (I-BVP). In order to use this method, one needs to impose a crucial restriction on the multi-patch configuration, namely, each patch must be a convex sub-domain. Since in the IgA framework patches are treated as mappings from the reference domain  $\widehat{\Omega} = (0, 1)^d$ , the estimation of local constants is reduced to the analysis of the IgA mapping and calculating the corresponding constant for  $\widehat{\Omega}$ .

The paper proceeds with the following structure. Section 2 formulates the general statement of the considered problem and recalls the definition of functional error estimates and their main properties in the context of reliable energy error estimation and efficient error-distribution indication. The next section serves as an overview of IgA techniques used in the current work, i.e., B-splines, NURBS, and THB-splines. In Section 4, we focus on the algorithms and details of the functional error estimates integration into the IgA framework. Last but not least, Section 5 presents the systematic selection of most relevant numerical examples and obtained results that illustrate numerical properties of studied error estimates and indicators.

## 2 Functional approach to the error control

In this section, we present a model problem, recall the well-posedness results for linear parabolic PDEs, which have been thoroughly studied in [33, 75, 73]. We also introduce functional a posteriori error estimates for the stated model and discuss its crucial properties.

Let  $\Omega \subset \mathbb{R}^d$ ,  $d = \{2, 3\}$ , be a bounded domain with Lipschitz boundary  $\Gamma := \partial\Omega$ . The elliptic BVP is formulated as

$$-\operatorname{div}(A\nabla u) = f \quad \text{in } \Omega, \quad (1)$$

$$u = 0 \quad \text{on } \Gamma, \quad (2)$$

where  $f$  supposed to be in  $L^2(\Omega)$ . Alternatively, the problem (1)–(2) can be viewed a system with two (primal and dual) unknowns

$$-\operatorname{div} \mathbf{p} = f \quad \text{in } \Omega, \quad (3)$$

$$\mathbf{p} = A\nabla u \quad \text{in } \Omega, \quad (4)$$

$$u = 0 \quad \text{on } \Gamma. \quad (5)$$

We assume that the operator  $A$  is symmetric and satisfies the condition of uniform ellipticity for almost all (a.a.)  $x \in \Omega$ , which reads

$$\underline{\nu}_A |\xi|^2 \leq A(x) \xi \cdot \xi \leq \bar{\nu}_A |\xi|^2, \quad \text{for all } \xi \in \mathbb{R}^d, \quad (6)$$

with  $0 < \underline{\nu}_A \leq \bar{\nu}_A < \infty$ . Throughout the paper, the following notation for the norms is used:

$$\|\boldsymbol{\tau}\|_{A, \Omega}^2 := (A\boldsymbol{\tau}, \boldsymbol{\tau})_\Omega, \quad \|\boldsymbol{\tau}\|_{A^{-1}, \Omega}^2 := (A^{-1}\boldsymbol{\tau}, \boldsymbol{\tau})_\Omega, \quad \text{for all } \boldsymbol{\tau} \in [L^2(\Omega)]^d,$$

where  $(A\mathbf{u}, \mathbf{v})_\Omega := \int_\Omega A\mathbf{u} \cdot \mathbf{v} \, dx$  stands for a weighted L2 scalar-product for all  $\mathbf{u}, \mathbf{v} \in [L^2(\Omega)]^d$ . After multiplying (1) by the test function

$$\eta \in H_0^1(\Omega) := \{u \in L^2(\Omega) \mid \nabla u \in L^2(\Omega), u|_\Gamma = 0\},$$

we arrive at the standard generalised formulation of (1)–(2): find  $u \in H_0^1(\Omega)$  satisfying the integral identity

$$a(u, \eta) := (A\nabla u, \nabla \eta)_\Omega = (f, \eta)_\Omega =: l(\eta), \quad \forall \eta \in H_0^1(\Omega). \quad (7)$$

According to [33], the generalised problem (7) has a unique solution in  $H_0^1(\Omega)$  provided that  $f \in L^2(\Omega)$  and condition (6) holds.

We consider the functional error estimates, which provide a guaranteed two-sided bound of the distance  $e := u - v$  between the generalised solution of (7)  $u$  and any function  $v \in H_0^1(\Omega)$ . It is important to emphasise that the suggested functional approach to error estimates' derivation is universal for any numerical method used to discretise bilinear form (7). This fact makes it rather unique in comparison with alternative approaches, which are always tailored to the discretised version of the identity  $a(u, \eta) = l(\eta)$ . Later on, the considered  $v$  is generated numerically, and the distance to  $u$  is evaluated in terms of the total energy norm

$$\|e\|_{\Omega}^2 := \|\nabla e\|_{A, \Omega}^2 \quad (8)$$

as well as its element-wise contributions  $\|\nabla e\|_{A, K}^2$  such that

$$\|e\|_{\Omega}^2 := \sum_{K \in \mathcal{K}_h} \|\nabla e\|_{A, K}^2.$$

Here,  $K$  represents the elements of the mesh  $\mathcal{K}_h$  introduced on  $\Omega$ . Hence, besides providing the guaranteed upper bound of total error (8), the majorant yields a quantitatively sharp indicator of the local error distribution.

**Remark 1** *It has been proved that the integrand of the majorant tends to the distribution of the true error in the sense of the measure, if the majorant globally converges (from above) to the true value of the error. In other words, the measure of the set, where the local difference between majorant and true error is bigger than a given epsilon, tends to zero. For the purposes of the error indication, it is enough ([52, Section 3]).*

To derive the upper bound, we need to transform (7) by subtracting  $a(v, \eta)$  from left- (LHS) and right-hand side (RHS) and by setting  $\eta = e$ . Thus, one obtains the error identity

$$\|e\|_{\Omega}^2 = (f, e)_{\Omega} - (A\nabla v, \nabla e)_{\Omega}. \quad (9)$$

The main idea of functional approach is the introduction of an auxiliary vector-valued variable

$$\mathbf{y} \in H(\Omega, \text{div}) := \left\{ \mathbf{y} \in [\mathbf{L}2(\Omega)]^d \mid \text{div} \mathbf{y} \in \mathbf{L}2(\Omega) \right\}$$

satisfying

$$(\text{div} \mathbf{y}, v)_{\Omega} + (\mathbf{y}, \nabla v)_{\Omega} = 0. \quad (10)$$

In further calculations, the above-introduced variable allows an additional degree of freedom for the majorant (additional optimisation step), whereas, for instance, the residual error estimates do not have this flexibility in improving its values. Next, we add the identity (10) to the RHS of (9), which yields

$$\|e\|_{\Omega}^2 = (f + \text{div} \mathbf{y}, e)_{\Omega} + (\mathbf{y} - A\nabla v, \nabla e)_{\Omega}. \quad (11)$$

The *equilibrated* and *dual residual-functionals* obtained in the RHS of (11) mimic equations (3) and (4), respectively, and are denoted by

$$\mathbf{r}_{\text{eq}}(v, \mathbf{y}) := f + \text{div} \mathbf{y} \quad \text{and} \quad \mathbf{r}_{\text{d}}(v, \mathbf{y}) := \mathbf{y} - A\nabla v. \quad (12)$$

**Theorem 1** (a) *For any functions  $v \in H_0^1(\Omega)$  and  $\mathbf{y} \in H(\Omega, \text{div})$ , we have the estimate*

$$\|e\|_{\Omega}^2 \leq \overline{\mathbf{M}}^2(v, \mathbf{y}; \beta) := (1 + \beta) \|\mathbf{r}_{\text{d}}\|_{A^{-1}, \Omega}^2 + (1 + \frac{1}{\beta}) \frac{C_{\text{F}\Omega}^2}{\underline{\nu}_A} \|\mathbf{r}_{\text{eq}}\|_{\Omega}^2, \quad (13)$$

where the residuals  $\mathbf{r}_{\text{d}}$  and  $\mathbf{r}_{\text{eq}}$  are defined in (12),  $\beta$  is a positive parameter, and  $C_{\text{F}\Omega}$  is the constant in the Friedrichs inequality [18]

$$\|v\|_{\Omega} \leq C_{\text{F}\Omega} \|\nabla v\|_{\Omega}, \quad \forall v \in H_0^1(\Omega).$$

(b) *For  $\beta > 0$ , the variational problem*

$$\inf_{\substack{v \in H_0^1(\Omega) \\ \mathbf{y} \in H(\Omega, \text{div})}} \overline{\mathbf{M}}(v, \mathbf{y}; \beta)$$

has a solution (with the corresponding zero-value for the functional), and its minimum is attained if and only if  $v = u$  and  $\mathbf{y} = A\nabla u$ .

**Proof:** For the detailed proof of this theorem we refer the reader to [53, Section 3.2].  $\square$

For the real-life problems, the exact solution is usually not known, therefore evaluation of  $\|e\|_{\Omega}^2$  becomes impossible. For the efficiency verification of  $\bar{M}^2(v, \mathbf{y}; \beta)$ , the lower bound of the error (further also referred as minorant) has been derived using variational arguments (see Theorem 2).

**Theorem 2** For any functions  $v, w \in H_0^1(\Omega)$ , we have the estimate

$$\|e\|_{\Omega}^2 \geq \sup_{w \in H_0^1(\Omega)} \bar{M}^2(v, w) := 2(J(v) - J(w)), \quad J(v) := (f, v) - \frac{1}{2} \|\nabla v\|_{\Omega}^2, \quad (14)$$

where  $J(v)$  is the variational functional of the problem (3)–(5).

**Proof:** For the detailed proof of this theorem, we refer the reader to [53, Section 4.1].  $\square$

Remarks below summarise several essential properties of the error estimate derived in Theorem 1.

**Remark 2** Each term on the RHS of (13) serves as the penalty of the error that might occur in equations (3) and (4). The positive weight  $\beta$  can be selected optimally in order to get the best value of the majorant. The constant  $C_{F\Omega}$  acts as a geometric characteristic for the considered domain  $\Omega$  (unlike, for instance, in the least-square methods, where the weights are selected after the terms  $\|\mathbf{r}_d\|_{A^{-1}, \Omega}^2$  and  $\|\mathbf{r}_{eq}\|_{\Omega}^2$  were calculated). From the author's point of view, this constant is essential and cannot be excluded since it scales proportionally to the diameter of the considered  $\Omega$ . Moreover, in order to guarantee the reliability of  $\bar{M}(v, \mathbf{y}; \beta)$ , the constant  $C_{F\Omega}$  must be estimated from above in a reliable way. Since in practice the term  $\|\mathbf{r}_{eq}\|_{\Omega}^2$  is rather small compared to the dominating term  $\|\mathbf{r}_d\|_{\Omega}^2$ , the Friedrichs constant can be replaced by some penalty constant  $C \geq C_{F\Omega}$  (even though it might affect the ratio of the majorant to the error). In what follows, to characterise the efficiency of (13), we use the quantity  $I_{\text{eff}}(\bar{M}) := \bar{M}/\|e\|_{\Omega}$  that measures the gap between  $\bar{M}(v, \mathbf{y}; \beta)$  and  $\|e\|_{\Omega}$ .

**Remark 3** The functional  $\bar{M}(v, \mathbf{y}; \beta)$  generates the upper bound of the error for any auxiliary  $\mathbf{y} \in H(\Omega, \text{div})$  and  $\beta > 0$ , therefore the choice of  $\mathbf{y}$  might vary. The first and most straightforward way to select this variable is to set  $\mathbf{y} = \mathcal{G}(A \nabla v)$ , where  $\mathcal{G} : [L^2(\Omega)]^d \rightarrow H(\Omega, \text{div})$  is a certain gradient-averaging operator. For this case, using the IgA framework becomes quite advantageous since for splines of the degree  $p \geq 2$  an obtained  $v$  is a  $C^1$ -continuous function and  $\nabla v$  is already in  $H(\Omega, \text{div})$ . Therefore, no additional post-processing is needed. On the other hand, due to the quadratic structure of the majorant, it is rather obvious that the optimal error estimate value is achieved at  $\mathbf{y} = A \nabla u$ , i.e.,

$$\|\nabla e\|_{A, \Omega}^2 \leq \bar{M}(v, \nabla u) = (1 + \beta) \|\nabla e\|_{A, \Omega}^2 + C_{F\Omega}^2 (1 + \frac{1}{\beta}) \|f + \text{div}(\nabla u)\|_{\Omega}^2 = (1 + \beta) \|\nabla e\|_{A, \Omega}^2. \quad (15)$$

From (15), it is easy to see that if the auxiliary  $\mathbf{y}$  is chosen optimally and  $\beta$  is set to zero (in the RHS of (15)), there is no gap between  $\bar{M}$  and  $\|\nabla e\|_{A, \Omega}^2$ .

One of the numerical methods providing an efficient reconstruction of both dual and primal variables is a mixed method. It generates an efficient approximation of the pair  $(v, \mathbf{y}) \in W := H_0^1(\Omega) \times H(\Omega, \text{div})$  that can be straightforwardly substituted into the majorant  $\bar{M}(v, \mathbf{y})$ . Moreover, if the error is measured in terms of the combined norm, i.e., including the norm of the error in primal and in dual variables

$$\|(u, \mathbf{p}) - (v, \mathbf{y})\|_W := (\|\nabla(u - v)\|_{\Omega}^2 + \|\mathbf{p} - \mathbf{y}\|_{\Omega}^2 + \|\text{div}(\mathbf{p} - \mathbf{y})\|_{\Omega}^2)^{1/2},$$

it is controlled by the residuals of the majorant as follows:

$$\frac{1}{\sqrt{3}} (\|\mathbf{r}_d\|_{A^{-1}, \Omega} + \frac{1}{\sqrt{\mathcal{L}_A}} \|\mathbf{r}_{eq}\|_{\Omega}) \leq \|(u, \mathbf{p}) - (v, \mathbf{y})\|_W \leq \|\mathbf{r}_d\|_{A^{-1}, \Omega} + (1 + 2 \frac{C_{F\Omega}^2}{\mathcal{L}_A})^{1/2} \|\mathbf{r}_{eq}\|_{\Omega}.$$

We note that the ratio between the majorant  $\|\mathbf{r}_d\|_{A^{-1}, \Omega} + \frac{1}{\sqrt{\mathcal{L}_A}} \|\mathbf{r}_{eq}\|_{\Omega}$  (that does not include any constants) and the error  $\|(u, \mathbf{p}) - (v, \mathbf{y})\|_W$  is controlled by  $\sqrt{3}$ , which proves the robustness of such error estimate. The series of works (see, e.g., [56, 58, 57]) has confirmed the efficiency of combination of mixed methods and functional error estimates.

The alternative approach providing an accurate  $\mathbf{y}$ -reconstruction follows from the minimisation problem

$$\{\mathbf{y}_{\min}, \beta_{\min}\} := \arg \inf_{\beta > 0} \inf_{\mathbf{y} \in H(\Omega, \text{div})} \bar{M}(v, \mathbf{y}; \beta). \quad (16)$$

The latter one is equivalent to the variational formulation for the optimal  $\mathbf{y}_{\min}$ , i.e.,

$$\frac{C_{F\Omega}^2}{\beta_{\min}} (\text{div} \mathbf{y}_{\min}, \text{div} \mathbf{w})_{\Omega} + (A^{-1} \mathbf{y}_{\min}, \mathbf{w})_{\Omega} = - \frac{C_{F\Omega}^2}{\beta_{\min}} (f, \text{div} \mathbf{w})_{\Omega} + (A \nabla v, \mathbf{w})_{\Omega}, \quad \forall \mathbf{w} \in H(\Omega, \text{div}),$$

where the optimal  $\beta$  is given by  $\beta_{\min} := \frac{C_{\text{F}\Omega} \bar{m}_f}{\bar{m}_d}$  with

$$\bar{m}_f := \|\mathbf{r}_{\text{eq}}\|_{\Omega} \quad \text{and} \quad \bar{m}_d := \|\mathbf{r}_d\|_{A^{-1}, \Omega}. \quad (17)$$

In this work, using the IgA approximation schemes' setting, we apply the second method of the efficient  $\mathbf{y}$ -reconstruction described in detail in Section 4. To compare the performance of  $\bar{M}$  with alternative error estimates we use the standard residual error estimator (applied, e.g., in [20])

$$\bar{\eta}^2 = \sum_{K \in \mathcal{K}_h} \bar{\eta}_K^2, \quad \bar{\eta}_K^2 := h_K^2 \|f + \text{div}(A \nabla u_h)\|_{L^2(K)}^2, \quad (18)$$

where  $h_K$  denotes the diameter of cell  $K$ , and  $u_h$  stands for approximation reconstructed by the IgA scheme. The term measuring the jumps across the element edges, which is usually included into residual error estimates, vanishes in (18) due to the properties of  $u_h$  produced by the IgA schemes. It is provided in the G+Smo package and can be accessed by using the class available from the G+Smo library [38, `stable/src/gsErrEstPoissonResidual.h`].

### 3 IgA overview: B-splines, NURBS, and THB-splines

For the consistency of exposition, we first give an overview of the general IgA framework, the definitions of B-splines, NURBS, and THB-splines, their use in the geometrical representation of the computational domain  $\Omega$  and in the construction of IgA discretisation spaces.

Let  $p \geq 2$  denote the degree of polynomials used for the IgA approximations, and let  $n$  be the number of basis functions used to construct a B-spline curve. The *knot-vector* in  $\mathbb{R}$  is a non-decreasing set of coordinates in the parameter domain, written as  $\Xi = \{\xi_1, \dots, \xi_{n+p+1}\}$ ,  $\xi_i \in \mathbb{R}$ , where  $\xi_1 = 0$  and  $\xi_{n+p+1} = 1$ . The knots can be repeated, and the multiplicity of the  $i$ -th knot is indicated by  $m_i$ . Throughout the paper, we consider only open knot vectors, i.e.,  $m_1 = m_{n+p+1} = p + 1$ . For the one-dimensional parametric domain  $\hat{\Omega} := (0, 1)$ ,  $\hat{\mathcal{K}}_h := \{\hat{K}\}$  denotes a locally quasi-uniform mesh, where each element  $\hat{K} \in \hat{\mathcal{K}}_h$  is constructed by distinct neighbouring knots. The global size of  $\hat{\mathcal{K}}_h$  is denoted by

$$\hat{h} := \max_{\hat{K} \in \hat{\mathcal{K}}_h} \{\hat{h}_{\hat{K}}\}, \quad \text{where} \quad \hat{h}_{\hat{K}} := \text{diam}(\hat{K}).$$

Henceforth, we assume locally quasi-uniform meshes, i.e., the ratio of two neighbouring elements  $\hat{K}_i$  and  $\hat{K}_j$  satisfies the inequality

$$c_1 \leq \frac{\hat{h}_{\hat{K}_i}}{\hat{h}_{\hat{K}_j}} \leq c_2, \quad \text{where} \quad c_1, c_2 > 0.$$

The *univariate B-spline basis functions*  $\hat{B}_{i,p} : \hat{\Omega} \rightarrow \mathbb{R}$  are defined by means of the Cox-de Boor recursion formula

$$\hat{B}_{i,p}(\xi) := \frac{\xi - \xi_i}{\xi_{i+p} - \xi_i} \hat{B}_{i,p-1}(\xi) + \frac{\xi_{i+p+1} - \xi}{\xi_{i+p+1} - \xi_{i+1}} \hat{B}_{i+1,p-1}(\xi), \quad \hat{B}_{i,0}(\xi) := \begin{cases} 1 & \text{if } \xi_i \leq \xi < \xi_{i+1} \\ 0 & \text{otherwise} \end{cases}, \quad (19)$$

where a division by zero is defined to be zero. The B-splines are  $(p - m_i)$ -times continuously differentiable across the  $i$ -th knot with multiplicity  $m_i$ . Hence, if  $m_i = 1$  for inner knots, the B-splines of the degree e.o.c. are  $C^{p-1}$  continuous across them.

The *multivariate B-splines* on the parameter domain  $\hat{\Omega} := (0, 1)^d$ ,  $d = \{1, 2, 3\}$ , are defined as tensor products of the corresponding univariate ones. In the multidimensional case, we define a knot-vector dependent on the coordinate direction  $\Xi^\alpha = \{\xi_1^\alpha, \dots, \xi_{n^\alpha+p^\alpha+1}^\alpha\}$ ,  $\xi_i^\alpha \in \mathbb{R}$ , where  $\alpha = 1, \dots, d$  indicates the direction (in space or time). Furthermore, we introduce a set of multi-indices

$$\mathcal{I} = \{\mathbf{i} = (i_1, \dots, i_d) : i_\alpha = 1, \dots, n_\alpha, \quad \alpha = 1, \dots, d\}$$

and a multi-index  $\mathbf{p} := (p_1, \dots, p_d)$  indicating the order of polynomials. The tensor-product of univariate B-spline basis functions generates multivariate B-spline basis functions

$$\hat{B}_{\mathbf{i}, \mathbf{p}}(\boldsymbol{\xi}) := \prod_{\alpha=1}^d \hat{B}_{i_\alpha, p_\alpha}(\xi^\alpha), \quad \text{where} \quad \boldsymbol{\xi} = (\xi^1, \dots, \xi^d) \in \hat{\Omega}. \quad (20)$$

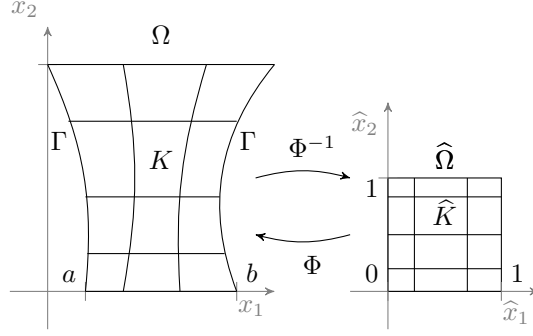


Figure 1: Mapping of  $\widehat{\Omega}$  to  $\Omega$ .

The *univariate and multivariate NURBS basis functions* are defined in a parametric domain by means of B-spline basis functions, i.e., for a given  $\mathbf{p}$  and any  $\mathbf{i} \in \mathcal{I}$ , NURBS basis functions are defined as  $\widehat{R}_{\mathbf{i}, \mathbf{p}} : \widehat{\Omega} \rightarrow \mathbb{R}$

$$\widehat{R}_{\mathbf{i}, \mathbf{p}}(\boldsymbol{\xi}) := \frac{w_{\mathbf{i}} \widehat{B}_{\mathbf{i}, \mathbf{p}}(\boldsymbol{\xi})}{\sum_{\mathbf{i} \in \mathcal{I}} w_{\mathbf{i}} \widehat{B}_{\mathbf{i}, \mathbf{p}}(\boldsymbol{\xi})}, \quad (21)$$

where  $w_{\mathbf{i}} \in \mathbb{R}^+$ . To recall basic definitions related to THB-splines, we follow the structure outlined in [20] and consider a finite sequence of nested  $d$ -variate tensor-product spline spaces  $\widehat{V}^0 \subset \widehat{V}^1 \subset \dots \subset \widehat{V}^N$  defined on the axis aligned box-domain  $\widehat{\Omega}^0 \subset \mathbb{R}^d$ . To each space  $V^\ell$  we assign a tensor-product B-spline basis of degree  $\mathbf{p}$

$$\{\widehat{B}_{\mathbf{i}, \mathbf{p}}^\ell\}_{\mathbf{i} \in \mathcal{I}^\ell}, \quad \mathcal{I}^\ell := \{\mathbf{i} = (i_1, \dots, i_d), \quad i_k = 1, \dots, n_k^\ell \text{ for } k = 1, \dots, d\},$$

where  $\mathcal{I}^\ell$  is a set of multi-indices for each level, and  $n_k^\ell$  denotes the number of univariate B-spline basis functions in the  $k$ -th coordinate direction. After assuming that  $\mathcal{I}^\ell$  has a fixed ordering and rewriting the basis as  $\widehat{\mathbf{B}}^\ell(\boldsymbol{\xi}) = (\widehat{B}_{\mathbf{i}, \mathbf{p}}^\ell(\boldsymbol{\xi}))_{\mathbf{i} \in \mathcal{I}^\ell}$ , it can be considered as a column-vector of basis functions. Then, a spline function  $s : \widehat{\Omega}^0 \rightarrow \mathbb{R}^m$  is defined by  $\widehat{\mathbf{B}}^\ell(\boldsymbol{\xi})$  and a coefficient matrix  $C^\ell$ , i.e.,

$$s(\boldsymbol{\xi}) = \sum_{\mathbf{i} \in \mathcal{I}^\ell} \widehat{B}_{\mathbf{i}, \mathbf{p}}^\ell(\boldsymbol{\xi}) c_{\mathbf{i}}^\ell = \widehat{\mathbf{B}}^\ell(\boldsymbol{\xi})^\top C^\ell,$$

where  $c_{\mathbf{i}}^\ell \in \mathbb{R}^m$  are row-coefficients of  $C^\ell$ .

Since  $\widehat{V}^\ell \subset \widehat{V}^{\ell+1}$ , the basis  $\widehat{\mathbf{B}}^\ell$  can be represented by the linear combination of  $\widehat{\mathbf{B}}^{\ell+1}$ , namely,

$$s(\boldsymbol{\xi}) = \widehat{\mathbf{B}}^\ell(\boldsymbol{\xi})^\top C^\ell = \widehat{\mathbf{B}}^{\ell+1}(\boldsymbol{\xi})^\top R^{\ell+1} C^\ell,$$

where  $R^{\ell+1}$  is a refinement matrix. Its entries can be obtained from B-splines refinement rules (see [49]). Along with nested space, a corresponding sequence of nested domains is considered

$$\widehat{\Omega}^0 \supseteq \widehat{\Omega}^1 \supseteq \dots \supseteq \widehat{\Omega}^N, \quad (22)$$

where each  $\widehat{\Omega}^\ell \in \mathbb{R}^d$  is covered by a collection of cells with respect to the tensor-product grid of level  $l$ . In this work, we focus on dyadic cell refinement for the bi- and trivariate cases with uniform degrees  $p_\alpha = p$  for all levels and coordinate directions, therefore,  $\mathbf{p} = p$  in further exposition.

Let the *characteristic matrix*  $X^\ell$  of  $\widehat{\mathbf{B}}^\ell(\boldsymbol{\xi})$  w.r.t. domains  $\Omega^\ell$  and  $\Omega^{\ell+1}$  is defined as

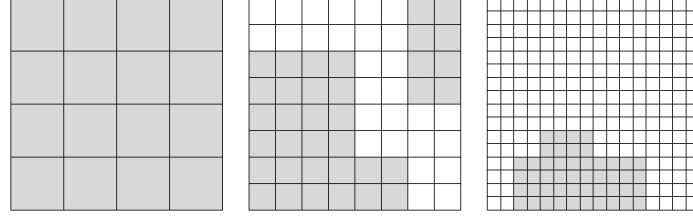
$$X^\ell := \text{diag}(x_{\mathbf{i}}^\ell)_{\mathbf{i} \in \mathcal{I}^\ell}, \quad x_{\mathbf{i}}^\ell := \begin{cases} 1, & \text{if } \text{supp} \widehat{B}_{\mathbf{i}, \mathbf{p}}^\ell \subseteq \Omega^\ell \wedge \text{supp} \widehat{B}_{\mathbf{i}, \mathbf{p}}^\ell \not\subseteq \Omega^{\ell+1} \\ 0, & \text{otherwise.} \end{cases}$$

Next, for each level  $\ell$ , the set of the indices of *active functions* can be defined with  $\mathcal{I}_*^\ell := \{\mathcal{I}^\ell : x_{\mathbf{i}}^\ell = 1\}$ . To store the indices of all active functions at all hierarchical levels, we define an *index set*

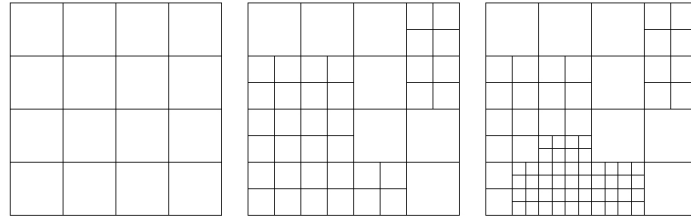
$$\mathcal{I} := \{(\ell, \mathbf{i}) : \ell \in \{0, \dots, N\}, \mathbf{i} \in \mathcal{I}_*^\ell\}.$$

The initial hierarchical data structure defined by the tensor-product mesh  $\widehat{\Omega}^0$  (see Figure 2a). In particular, we illustrate the knot lines of the spaces  $V^0 \subset V^1 \subset V^2$  (where levels increase from the left to the right). By means

of the insertion operation, new subdomains can be added to obtain new representations  $\widehat{\Omega}^0 \supseteq \widehat{\Omega}^1 \supseteq \widehat{\Omega}^2$ . The sets of active basis functions  $\mathcal{I}_*^\ell$  as well as the characteristic matrices  $X^\ell$  for all levels  $\ell$  are extracted simultaneously with the new box insertion and initialisation of the basis. Figure illustrates meshes at the refinement levels  $\ell = 0, 1, 2$ .



(a) Knot lines and inserted subdomain (shaded)



(b) Hierarchical meshes for refinement levels

Figure 2: Bivariate configuration for hierarchical levels  $\ell = 0, 1, 2$  (the picture is taken from [20]).

The THB-spline basis related to the hierarchical domains is defined as

$$\widehat{\mathbf{T}}(\boldsymbol{\xi}) = (\mathcal{K}_i^\ell(\boldsymbol{\xi}))_{(l,i) \in \mathcal{I}}, \quad \mathcal{K}_i^\ell(\boldsymbol{\xi}) = \text{trunc}^N(\text{trunc}^{N-1}(\dots \text{trunc}^{\ell+1}(\widehat{B}_{i,p}^\ell(\boldsymbol{\xi})))),$$

where the *truncation* of any function  $s(\boldsymbol{\xi}) \in \widehat{V}^\ell$  w.r.t. level  $\ell + 1$  is defined by

$$\text{trunc}^{\ell+1}(s(\boldsymbol{\xi})) = \widehat{\mathbf{B}}^{\ell+1}(\boldsymbol{\xi})^\top (I^{\ell+1} - X^{\ell+1}) R^{\ell+1} C^\ell.$$

Here,  $I^{\ell+1}$  denotes an identity matrix  $I^{\ell+1}$  of size  $|I^{\ell+1}| \times |I^{\ell+1}|$ , the multiplication of  $R^{\ell+1}$  by  $C^\ell$  represents  $s(\boldsymbol{\xi})$  w.r.t. to the level  $\ell + 1$ , and additional multiplication by  $(I^{\ell+1} - X^{\ell+1})$  performs the truncation operation. For the detailed discussion of truncation operation, we refer the reader to [21, 22, 20]. We illustrate an effect of the truncation for the case of univariate quadratic spline basis functions (see Figure 3). Figure 3a presents the HB-splines for the hierarchical levels  $\ell = 2, 3, 4$ , whereas Figure 3b shows the same levels for THB-splines. On the last row, basis functions influenced by the truncation on coarser levels are exposed, i.e., THB-splines before and after being truncated are denoted by the grey and black marker, respectively.

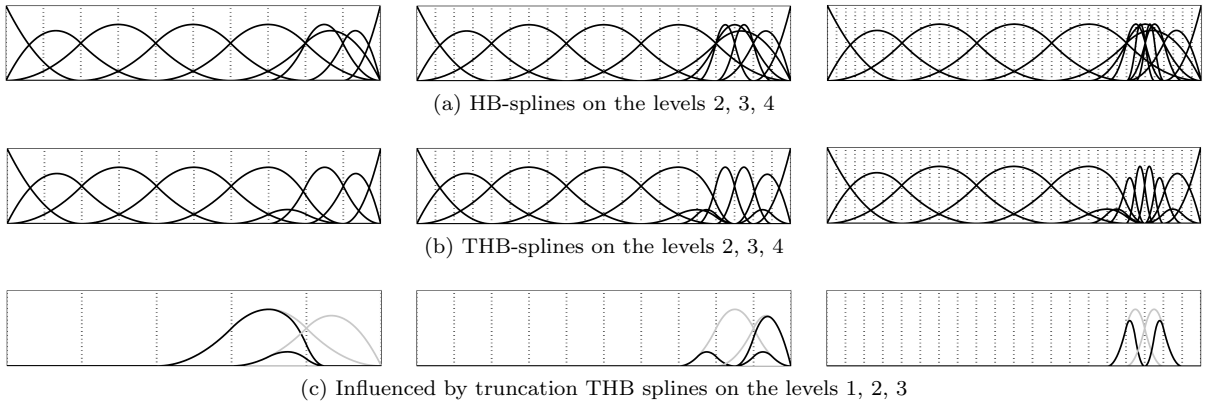


Figure 3: Comparison of HB- and THB-splines on the different refinement levels (the picture is taken from [20]).

The physical domain  $\Omega \subset \mathbb{R}^d$  is defined by the geometrical mapping of the parametric domain  $\widehat{\Omega} := (0, 1)^d$ :

$$\Phi : \widehat{\Omega} \rightarrow \Omega := \Phi(\widehat{\Omega}) \subset \mathbb{R}^d, \quad \Phi(\boldsymbol{\xi}) := \sum_{i \in \mathcal{I}} \widehat{\mathcal{B}}_{i,p}(\boldsymbol{\xi}) c_i, \quad (23)$$

where  $c_i \in \mathbb{R}^d$  are control points, and  $\widehat{\mathcal{B}}_{i,p}$  stands for either B-splines, NURBS, or THB-basis functions. The mesh  $\mathcal{K}_h$  discretising  $\Omega$  consists of elements  $K \in \mathcal{K}_h$  that are the images of  $\widehat{K} \in \widehat{\mathcal{K}}_h$ , i.e.,

$$\mathcal{K}_h := \{K = \Phi(\widehat{K}) : \widehat{K} \in \widehat{\mathcal{K}}_h\}.$$

The global mesh-size is denoted by

$$h := \max_{K \in \mathcal{K}_h} \{h_K\}, \quad h_K := \|\nabla \Phi\|_{\mathbf{L}^\infty(K)} \widehat{h}_{\widehat{K}}. \quad (24)$$

Moreover, we assume that  $\mathcal{K}_h$  is a quasi-uniform mesh, i.e., there exists a positive constant  $C_u$  independent of  $h$ , such that  $h_K \leq h \leq C_u h_K$ .

## 4 Functional error estimates within the IgA framework

In this section, we present the algorithms used for general reliable computations and functional-type error estimates reconstruction. Then we proceed with commenting on the implementation of these error estimates in G+Smo and their integration into the library's structure. Finally, we present a series of examples demonstrating numerical properties of derived error majorants.

### 4.1 Reliable reconstruction of IgA approximations. Algorithms

In order to keep the presentation concise, we restrict (3)–(5) to the Dirichlet–Poisson problem

$$-\Delta u = f \quad \text{in } \Omega := (0, 1)^d \in \mathbb{R}^d, \quad d = \{2, 3\}, \quad u = 0 \quad \text{on } \Gamma = \partial\Omega. \quad (25)$$

Let the approximation

$$u_h \in V_{0h} := V_h \cap H_0^1(\Omega), \quad \text{where } V_h \equiv \mathcal{S}_h^{p,p} := \{\phi_{h,i}^{(p)} := \widehat{V}_h \circ \Phi^{-1}\}.$$

Here,  $\widehat{V}_h \equiv \widehat{\mathcal{S}}_h^{p,p}$  is generated with NURBS of degree  $p$ , i.e.,  $\widehat{V}_h := \text{span} \{\widehat{\mathcal{B}}_{i,p}\}_{i \in \mathcal{I}}$ . Due to the one-patch setting and restriction on the knots' multiplicity of  $\widehat{\mathcal{S}}_h^{p,p}$ , the smoothness  $u_h \in C^{p-1}$  is automatically provided. Since no numerical algorithms specific to the hierarchical levels of the localised splines will be discussed below, we use the same notation for spaces generated by THB-splines. Therefore, the constructed approximation can be written as

$$u_h(x) = u_h(x_1, \dots, x_d) := \sum_{i \in \mathcal{I}} \underline{u}_{h,i} \phi_{h,i}^{(p)}(x),$$

where  $\underline{u}_h := [\underline{u}_{h,i}]_{i \in \mathcal{I}} \in \mathbb{R}^{|\mathcal{I}|}$  is a vector of degrees of freedom (d.o.f.) defined by the system

$$\mathbf{K}_h^{(p)} \underline{u}_h = \mathbf{f}_h^{(p)}, \quad \mathbf{K}_h^{(p)} := [(\nabla \phi_{h,i}^{(p)}, \nabla \phi_{h,j}^{(p)})_\Omega]_{i,j \in \mathcal{I}}, \quad \mathbf{f}_h^{(p)} := [(f, \phi_{h,i}^{(p)})_\Omega]_{i \in \mathcal{I}}. \quad (26)$$

The majorant corresponding to the problem (25) reads as

$$\overline{\mathbf{M}}^2(u_h, \mathbf{y}_h) := (1 + \beta) \overline{\mathbf{m}}_d^2 + (1 + \frac{1}{\beta}) C_{\text{F}\Omega}^2 \overline{\mathbf{m}}_{\text{eq}}^2 = (1 + \beta) \|\mathbf{y}_h - \nabla u_h\|_\Omega^2 + (1 + \frac{1}{\beta}) C_{\text{F}\Omega}^2 \|\text{div} \mathbf{y}_h + f\|_\Omega^2, \quad (27)$$

where  $\overline{\mathbf{m}}_f$  and  $\overline{\mathbf{m}}_d$  are defined in (17),  $\beta > 0$  and  $\mathbf{y}_h \in Y_h \subset H(\Omega, \text{div})$ . Here, the approximation space for

$$\mathbf{y}_h \in Y_h \equiv \oplus^d \mathcal{S}_h^{q,q} \equiv \mathcal{S}_h^{q,q} \oplus \dots \oplus \mathcal{S}_h^{q,q} := \{\widehat{Y}_h \circ \Phi^{-1}\}$$

is generated by the push-forward of a corresponding space in the parametric domain

$$\widehat{Y}_h := \oplus^d \widehat{\mathcal{S}}_h^{q,q} \equiv \widehat{\mathcal{S}}_h^{q,q} \oplus \dots \oplus \widehat{\mathcal{S}}_h^{q,q}.$$

Here,  $\widehat{\mathcal{S}}_h^{q,q}$  is a space of NURBS with the degree  $q$  for each of  $d$  components of  $\mathbf{y}_h = (y_h^{(1)}, \dots, y_h^{(d)})^\top$ . The details of the numerical reconstruction of (27) were thoroughly studied in [28]. The best estimate follows from the optimisation of  $\overline{\mathbf{M}}(u_h, \mathbf{y}_h)$  w.r.t. function

$$\mathbf{y}_h(x) := \sum_{i \in \mathcal{I}} \underline{\mathbf{y}}_{h,i} \psi_{h,i}(x).$$

The basis functions  $\psi_{h,i}$  generate the space  $Y_h$ , whereas  $\underline{\mathbf{y}}_h := [\underline{\mathbf{y}}_{h,i}]_{i \in \mathcal{I} \times d} \in \mathbb{R}^{d|\mathcal{I}|}$  is a vector of d.o.f of  $\mathbf{y}_h$  defined by a system

$$(C_{\text{F}\Omega}^2 \text{Div}_h + \beta \text{M}_h) \underline{\mathbf{y}}_h = -C_{\text{F}\Omega}^2 z_h + \beta g_h, \quad (28)$$

where

$$\begin{aligned} \text{Div}_h &:= [(\text{div} \psi_i, \text{div} \psi_j)_\Omega]_{i,j=1}^{d|\mathcal{I}|}, & z_h &:= [(f, \text{div} \psi_j)_\Omega]_{j=1}^{d|\mathcal{I}|}, \\ \text{M}_h &:= [(\psi_i, \psi_j)_\Omega]_{i,j=1}^{d|\mathcal{I}|}, & g_h &:= [(\nabla v, \psi_j)_\Omega]_{j=1}^{d|\mathcal{I}|}. \end{aligned}$$

According to the numerical results obtained in [28], the most efficient majorant reconstruction (with uniform refinement) is obtained when  $q$  is set substantially higher than  $p$ . Let us assume that  $q = p + m$ ,  $m \in \mathbb{N}^+$ . At the same time, when  $u_h$  is reconstructed on the mesh  $\mathcal{K}_h$ , we use a coarser one  $\mathcal{K}_{Mh}$ ,  $M \in \mathbb{N}^+$  in order to recover  $\mathbf{y}_h$ . For the reader's convenience, all used notation is summarised in Table 1. The initial mesh  $\mathcal{K}_h^0$  and the basis functions defined on it are assumed to be given via the geometry representation of the computational domain. The exact representation of geometry on the initial (the coarsest) level is preserved in the process of mesh refinement.

For the reconstruction of  $\underline{\mathbf{M}}(v, w)$ , let the approximation

$$w_h \in W_{0h} := W_h \cap H_0^1(\Omega), \quad \text{where } W_h \equiv \mathcal{S}_h^{r,r} := \{\varphi_{h,i}^r := \widehat{W}_h \circ \Phi^{-1}\}.$$

Here,  $\widehat{W}_h \equiv \widehat{\mathcal{S}}_h^{r,r}$  is approximation space generated with NURBS of degree  $r$  on the parameter domain, i.e.,  $\widehat{W}_h := \text{span} \{\widehat{\mathcal{B}}_{i,r}\}_{i \in \mathcal{I}}$ . Then, the auxiliary approximation can be written as

$$w_h(x) = w_h(x_1, \dots, x_d) := \sum_{i \in \mathcal{I}} \underline{w}_{h,i} \phi_{h,i}^{(r)},$$

where  $\underline{w}_h := [\underline{w}_{h,i}]_{i \in \mathcal{I}} \in \mathbb{R}^{|\mathcal{I}|}$  is a vector of degrees of freedom (d.o.f.) defined by the system

$$\mathbf{K}_h^{(r)} \underline{w}_h = \mathbf{f}_h^{(r)}, \quad \mathbf{K}_h^{(r)} := [(\nabla \varphi_{h,i}^{(r)}, \nabla \varphi_{h,j}^{(r)})_\Omega]_{i,j \in \mathcal{I}}, \quad \mathbf{f}_h^{(r)} := [(f, \varphi_{h,i}^{(r)})_\Omega]_{i \in \mathcal{I}}. \quad (29)$$

Analogously to the selection of the  $q$  for the space  $Y_h$ , we let  $r = p + l$ ,  $l \in \mathbb{N}^+$ . At the same time, we use a coarser mesh  $\mathcal{K}_{Lh}$ ,  $L \in \mathbb{N}^+$  for the  $w_h$  approximation.

The classical strategy of the reliable  $u_h$ -approximation is summarised in Algorithm 1. Let us assume that the problem data such as  $f$ ,  $u_0$ , and  $\Omega$  of (3)–(5) are provided. The Input of Algorithm 1 is the initial mesh  $\mathcal{K}_h$  (or the one obtained on the previous refinement step). It provides the refined version of  $\mathcal{K}_h$  denoted by  $\mathcal{K}_{h_{\text{ref}}}$  as an output. The process of new mesh generation can be divided into classical block-chain, i.e.,

APPROXIMATE  $\rightarrow$  ESTIMATE  $\rightarrow$  MARK  $\rightarrow$  REFINE.

On the APPROXIMATE step, we construct the system that provides the d.o.f. of  $u_h$ , i.e., we assemble the matrix  $\mathbf{K}_h^{(p)}$  and RHS  $\mathbf{f}_h^{(p)}$  defined in (26), and solve it with a direct sparse LDL<sup>T</sup> Cholesky factorisations for  $d = 2$  and conjugate gradient (CG) method for  $d = 3$ . In the follow-up report, we will investigate how the selection of the initial guess enhances the performance of the iterative solver. In particular, we use the work [12, 5] that studies the so-called cascadic preconditioned conjugate gradient (CPCG) method. The latter one has an improved speed of convergence due to initial guess chosen as an interpolation of the approximation obtained on the previous refinement (hierarchical) level. It appears that such a cascadic structure of the meshes by itself realises some kind of preconditioning. The time spent on assembling and solving sub-procedures for  $u_h$  is tracked and saved in vectors  $t_{\text{as}}(u_h)$  and  $t_{\text{sol}}(u_h)$ , respectively. This notation is used in the upcoming examples to analyse the efficiency of Algorithm 1 and compare the computational costs for its blocks.

The next ESTIMATE step is first and foremost responsible for the reconstruction of global estimate  $\overline{\mathbf{M}}(u_h, \mathbf{y}_h)$  as well as the element-wise error indicator distribution  $\overline{\mathbf{m}}_d^2(u_h, \mathbf{y}_h)$  (see (17)) that follows. The time spent for this

---

$p$	degree of the splines used for $u_h$ approximation
$q$	degree of the splines used for $\mathbf{y}_h$ approximation
$r$	degree of the splines used for $w_h$ approximation
$m$	$q - p$
$l$	$r - p$
$S_h^{p,p} (S_h^{r,r})$	approximation space for the scalar-functions generated by splines
$\oplus^d S_h^{q,q}$	approximation space for the $d$ -dimensional vector-functions generated by splines
$S_h^{q,q} \oplus S_h^{q,q}$	approximation space for the two-dimensional vector-functions generated by splines
$M$	coarsening ratio of the global size of the mesh for $u_h$ approximation to the global size of the mesh for $\mathbf{y}_h$ reconstruction
$L$	coarsening ratio of the global size of the mesh for $u_h$ approximation to the global size of the mesh for $w_h$ reconstruction
$\mathcal{K}_h (\mathcal{K}_h^{u_h})$	mesh used for $u_h$ approximation
$\mathcal{K}_{Mh} (\mathcal{K}_h^{\mathbf{y}_h}, M = 1)$	mesh used for $\mathbf{y}_h$ reconstruction
$\mathcal{K}_{Lh} (\mathcal{K}_h^{w_h}, L = 1)$	mesh used for $w_h$ reconstruction
$N_{\text{ref}}$	number of uniform or adaptive refinement steps
$N_{\text{ref},0}$	number of initial refinement steps performed before testing
$\mathbb{M}_*(\theta)$	marking criterion $*$ with the parameter $\theta$

---

Table 1: Table of notations.

is measured by  $t_{\text{as}}(\mathbf{y}_h) + t_{\text{sol}}(\mathbf{y}_h)$ . Simultaneously with the upper bound, we reconstruct minorant  $\underline{\mathbb{M}}(u_h, w_h)$ , whereas the time spent for its reconstruction is tracked by  $t_{\text{as}}(w_h) + t_{\text{sol}}(w_h)$ . Their detailed description of latter estimates generation is presented in Algorithms 2 and 3.

In the chain-block MARK, we apply a marking criterion denoted by  $\mathbb{M}_*(\theta)$ . It provides an algorithm for defining the threshold  $\Theta_*$  for selecting those  $K \in \mathcal{K}_h$  for further refinement that satisfies the criterion

$$\overline{m}_{d,K}^2 \geq \Theta_*(\mathbb{M}_*(\theta)), \quad K \in \mathcal{K}_h.$$

In the G+smo library [38], several marking strategies are considered. The first criterion defines an ‘absolute threshold’, and it is denoted as **GARU** (an abbreviation for ‘greatest appearing residual utilisation’). The corresponding threshold reads as

$$\Theta_{\text{GARU}} := \theta \max_{K \in \mathcal{K}_h} \{\overline{m}_{d,K}^2\}, \quad \theta \in (0, 1).$$

The percentage of marked elements (dictated by this criterion) varies at each refinement step since  $\Theta_{\text{GARU}}$  considers only the absolute value of the largest local error, without taking into account the element-wise distribution of the error.

The second marking criterion defining the ‘relative threshold’ is denoted as  $\mathbb{M}_{\text{PUCA}}$ , where **PUCA** stands for ‘percent-utilising cutoff ascertainment’. The corresponding amount of elements selected for the refinement can be approximated as follows:

$$|\{K : \overline{m}_{d,K}^2 > \Theta_{\text{PUCA}}\}_{K \in \mathcal{K}_h}| \approx (1 - \theta) \cdot |\{K\}_{K \in \mathcal{K}_h}|, \quad \theta \in (0, 1).$$

For instance, if we let  $\theta = 0.7$ ,  $\Theta_{\text{PUCA}}$  is chosen such that  $\overline{m}_{d,K}^2 \geq \Theta_{\text{PUCA}}$  holds for 30% of elements.

Last and most widely used criterion is called bulk marking (also known as the Dörfler marking [15]) and is denoted as  $\mathbb{M}_{\text{BULK}}(\theta)$ . According to this marking strategy, we select the subset of elements from the collection  $\mathcal{K}_h$  that has been sorted w.r.t. element-wise contributions  $\overline{m}_{d,K}^2$ , i.e.,  $\mathcal{K}'_h \leftarrow \mathcal{K}_h^{\text{sort}} := \text{sort}_{\overline{m}_{d,K}^2} \{\mathcal{K}_h\}$ , until we satisfy

$$\sum_{K \in \mathcal{K}'_h} \overline{m}_{d,K}^2 \geq \Theta_{\text{BULK}} := (1 - \theta) \sum_{K \in \mathcal{K}_h} \overline{m}_{d,K}^2, \quad \theta \in (0, 1).$$

This way, we form a subset of elements which contains the highest indicated errors. The selection process stops when the error accumulated on previous steps exceeds the ‘bulk’ level (threshold) defined by  $\theta$ . In the case of uniform refinement, all elements of  $\mathcal{K}_h$  are marked for refinement (i.e.,  $\theta = 0$ ). If the numerical IgA scheme is implemented correctly, the error is supposed to decrease at least as  $O(h^p)$  (which is verified throughout the numerical tests in Section 5).

Finally, on the last REFINE step, we apply the refinement algorithm  $\mathcal{R}$  to those elements that have been selected on the MARK level. Since the THB-splines are based on the subdomains of different hierarchical levels,

---

**Algorithm 1** Reliable reconstruction of  $u_h$  (a single refinement step)

---

**Input:**  $\mathcal{K}_h$  {discretisation of  $\Omega$ }  
span  $\{\phi_{h,i}^{(p)}\}, i = 1, \dots, |\mathcal{I}|$   $\{V_h$ -basis}

**APPROXIMATE:**

- ASSEMBLE the matrix  $K_h^{(p)}$  and RHS  $f_h^{(p)}$  :  $\mathbf{t}_{\text{as}}(\mathbf{u}_h)$
- SOLVE  $K_h^{(p)} \underline{\mathbf{u}}_h = f_h^{(p)}$  :  $\mathbf{t}_{\text{sol}}(\mathbf{u}_h)$
- Reconstruct  $u_h = \sum_{i \in \mathcal{I}} \underline{\mathbf{u}}_i \phi_{h,i}^{(p)}(x)$

**ESTIMATE:** Reconstruct  $\overline{\mathbf{M}}(u_h, \mathbf{y}_h)$  and  $\overline{\mathbf{m}}_d^2(u_h, \mathbf{y}_h)$  :  $\mathbf{t}_{\text{as}}(\mathbf{y}_h) + \mathbf{t}_{\text{sol}}(\mathbf{y}_h)$

Reconstruct  $\underline{\mathbf{M}}(u_h, w_h)$  :  $\mathbf{t}_{\text{as}}(\mathbf{w}_h) + \mathbf{t}_{\text{sol}}(\mathbf{w}_h)$

**MARK:** Using the marking criteria  $\mathbf{M}_*(\theta)$ , select the elements  $K$  of mesh  $\mathcal{K}_h$  that must be refined

**REFINE:** Execute the refinement strategy:  $\mathcal{K}_{h_{\text{ref}}} = \mathcal{R}(\mathcal{K}_h)$

**Output:**  $\mathcal{K}_{h_{\text{ref}}}$  {refined discretisation of  $\Omega$ }

---

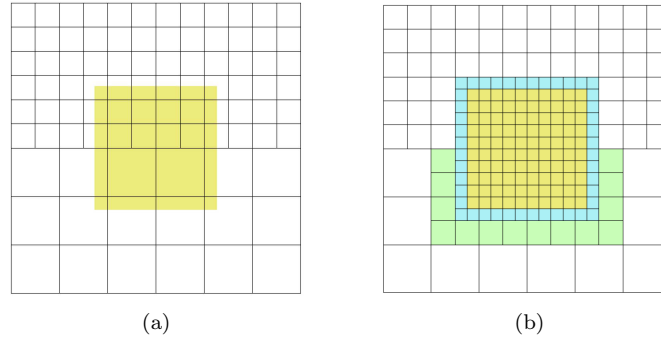


Figure 4: Example of the box insertion in the second hierarchical level of THB-spline (the picture is taken from [20]).

the procedure  $\mathcal{R}$  increases the level of subdomains that have been selected by  $\mathbf{M}_*(\theta)$ . For  $\mathcal{R}$ , a dyadic cell refinement is applied. To prevent the cases of refinement, when the inserted box is not aligned with the current hierarchical mesh (occurrence of the L-shaped cells), ‘affected’ cells of lower levels are locally subdivided to adapt to the inserted box. For that, in further examples, we specify the extension of the refined box by one cell (see, e.g., Figure 4). Here, Figure 4a illustrates the box insertion (yellow area) in the second hierarchical level of THB-spline. In Figure 4b, blue cells around the inserted box are the ‘one-cell’ extension of the yellow area. Green cells of the first level are the so-called ‘affected’ cells of zero level that have been locally subdivided to adapt to the inserted box.

Let us now consider the structure of Algorithm 2, which clarifies the ESTIMATE step of Algorithm 1 in the context of functional type error estimates. As the first Input argument, the algorithm receives the approximate solution  $u_h$  reconstructed with the IgA scheme. Since the majorant is minimised with respect to a vector-valued variable  $\mathbf{y}_h \in Y_h$ , the algorithm is also provided with the collection of basis functions generating the space  $Y_h := \text{span} \{\psi_{h,i}\}, i = 1, \dots, d|\mathcal{I}|$ . The last input parameter  $N_{\text{maj}}^{\text{it}}$  defines the number of the optimisation loops executed to obtain a good enough minimiser of  $\overline{\mathbf{M}}$ . According to the tests performed in [55] as well as experience of the author, one or two iterations are usually rather sufficient in order to achieve reasonable accuracy of error majorant. Technically, if the ratio between  $\overline{\mathbf{m}}_{\text{eq}}^2$  and  $\overline{\mathbf{m}}_d^2$  is small enough, the loop can be exited even if  $n < N_{\text{maj}}^{\text{it}}$ . This condition might cut the computational costs for the error control. However, for the consistency of exposition this is not incorporated into Algorithm 2 but only noted here as a remark.

It is crucial to emphasise that both matrices  $\text{Div}_h, \mathbf{M}_h$  and vectors  $z_h, \mathbf{g}_h$  are assembled only once and remain unchanged in the minimisation procedure. The loop is iterated  $N_{\text{maj}}^{\text{it}}$  times, where on each step the optimal  $\mathbf{y}_h^{(n)}$  and  $\beta^{(n)}$  are reconstructed. In our implementation, the optimality system for the flux (cf. (28)) is solved by direct sparse LDL<sup>T</sup> Cholesky factorisations for  $d = 2$  and by a conjugate gradient method for  $d = 3$  (again,

---

**Algorithm 2** ESTIMATE step (majorant reconstruction)

---

**Input:**  $u_h$  {approximation}  
 $\mathcal{K}_{Mh}$  {discretisation of  $\Omega$ },  
 $\text{span} \{ \boldsymbol{\psi}_{h,i} \}, i = 1, \dots, d|Z|$   $\{Y_h\text{-basis}\}$ ,  
 $N_{\text{maj}}^{\text{it}}$  {number of optimisation iterations}

**ASSEMBLE**  $\text{Div}_h, M_h \in \mathbb{R}^{d|Z| \times d|Z|}$  and  $\mathbf{z}_h, \mathbf{g}_h \in \mathbb{R}^{d|Z|}$  :  $\mathbf{t}_{\text{as}}(\mathbf{y}_h)$

Set  $\beta^{(0)} = 1$

**for**  $n = 1$  **to**  $N_{\text{maj}}^{\text{it}}$  **do**

**SOLVE**  $(C_{\text{F}\Omega}^2 / \beta^{(n-1)} \text{Div}_h + M_h) \underline{\mathbf{y}}_h^{(n)} = -C_{\text{F}\Omega}^2 / \beta^{(n-1)} \mathbf{z}_h + \mathbf{g}_h$  :  $\mathbf{t}_{\text{sol}}(\mathbf{y}_h)$

Reconstruct  $\mathbf{y}_h^{(n)} := \sum_{i \in \mathcal{I} \times d} \underline{\mathbf{y}}_{h,i}^{(n)} \boldsymbol{\psi}_{h,i}$

Compute  $\overline{\mathbf{m}}_d^{2,(n)} := \|f + \text{div} \mathbf{y}_h^{(n)}\|_{\Omega}^2$  and  $\overline{\mathbf{m}}_{\text{eq}}^{2,(n)} := \|\mathbf{y}_h^{(n)} - \nabla u_h\|_{\Omega}^2$

Compute  $\beta^{(n)} = \frac{C_{\text{F}\Omega} \overline{\mathbf{m}}_f^{(n)}}{\overline{\mathbf{m}}_d^{(n)}}$

**end for**

Compute  $\overline{\mathbf{M}}^2(u_h, \mathbf{y}_h^{(n)}; \beta^{(n)}) := (1 + \beta^{(n)}) \overline{\mathbf{m}}_{\text{eq}}^{2,(n)} + (1 + \frac{1}{\beta^{(n)}}) C_{\text{F}\Omega}^2 \overline{\mathbf{m}}_d^{2,(n)}$

**Output:**  $\overline{\mathbf{M}}$  {total error majorant on  $\Omega$ },  
 $\overline{\mathbf{m}}_d = \overline{\mathbf{m}}_d^{(n)}$  {indicator of error distribution over  $\mathcal{K}_h$ }

---



---

**Algorithm 3** ESTIMATE step (minorant reconstruction)

---

**Input:**  $u_h$  {approximation}  
 $\mathcal{K}_{Lh}$  {discretisation of  $\Omega$ },  
 $\text{span} \{ \phi_{h,i}^{(r)} \}, i = 1, \dots, |Z|$   $\{W_h\text{-basis}\}$

**ASSEMBLE**  $\mathbf{K}_h^{(r)} \in \mathbb{R}^{|\mathcal{I}| \times |\mathcal{I}|}$  and  $\mathbf{f}_h^{(r)} \in \mathbb{R}^{|\mathcal{I}|}$  :  $\mathbf{t}_{\text{as}}(\mathbf{w}_h)$

**SOLVE**  $\mathbf{K}_h^{(r)} \underline{\mathbf{w}}_h = \mathbf{f}_h^{(r)}$  :  $\mathbf{t}_{\text{sol}}(\mathbf{w}_h)$

Reconstruct  $w_h(x) = w_h(x_1, \dots, x_d) := \sum_{i \in \mathcal{I}} \underline{\mathbf{w}}_{h,i} \phi_{h,i}^{(r)}$

Compute  $\underline{\mathbf{M}}^2(u_h, w_h) := 2(f, u_h - w_h) - (\|\nabla u_h\|_{\Omega}^2 + \|\nabla w_h\|_{\Omega}^2)$

**Output:**  $\underline{\mathbf{M}}$  {total error minorant on  $\Omega$ }

---

the initial guess is reconstructed from the approximation obtained in the earlier refinement). The time spent on ASSEMBLE and SOLVE steps with regard to the system (28) is measured by  $\mathbf{t}_{\text{as}}(\mathbf{y}_h)$  and  $\mathbf{t}_{\text{sol}}(\mathbf{y}_h)$ , respectively, and compared to values  $\mathbf{t}_{\text{as}}(u_h)$  and  $\mathbf{t}_{\text{sol}}(u_h)$  in forthcoming numerical examples.

Algorithm 3 illustrates the sequence of steps for lower error bound reconstruction. Both assembling and solving are analogous to Algorithm 1 for the primal approximation, but use the basis  $\phi_{h,i}^r$  of higher regularity. At the same time, we use the mesh  $\mathcal{K}_{Lh}$  that is up to  $L$  times coarser than the mesh used for  $u_h$ . The time-efficiency of the minorant reconstruction is tracked by  $\mathbf{t}_{\text{as}}(\mathbf{w}_h)$  and  $\mathbf{t}_{\text{sol}}(\mathbf{w}_h)$  measurements and later compared to those related to  $u_h$  and  $\mathbf{y}_h$  approximation.

Besides the computational costs related to the assembling and solving of (26) and (28), we measure the time spent on the element-wise (e/w) evaluation of error, majorant, minorant, and the residual error estimator. They are denoted by  $t_{\text{e/w}}(\|\nabla e\|)$ ,  $t_{\text{e/w}}(\overline{\mathbf{M}})$ ,  $t_{\text{e/w}}(\underline{\mathbf{M}})$ , and  $t_{\text{e/w}}(\overline{\eta})$ , respectively.

## 5 Numerical examples

In the current section, we present a series of examples demonstrating the numerical properties of the error majorants discussed above. We start with relatively simple examples, in which we aim to introduce the main properties of majorant and, at the same time, familiarise the reader with the structure of performed numerical tests. This approach is intended to bring the focus to analysis in more complicated examples discussed further.

# ref.	$\ \nabla e\ _\Omega$	$\bar{M}$	$\bar{m}_d$	$\bar{m}_f$	$I_{\text{eff}}(\bar{M})$	$I_{\text{eff}}(\bar{\eta})$	e.o.c
(a) $\mathbf{y}_h \in S_{3h}^{5,5} \oplus S_{3h}^{5,5}$ ( $m = 3, M = 3$ )							
3	2.5648e-03	3.2806e-03	3.1546e-03	5.5974e-04	1.2791	11.0113	3.4565
5	1.5952e-04	1.9770e-04	1.9084e-04	3.0441e-05	1.2393	10.9580	2.3602
7	9.9673e-06	1.1974e-05	1.1921e-05	2.3799e-07	1.2013	10.9546	2.0901
9	6.2294e-07	7.4549e-07	7.4502e-07	2.0851e-09	1.1967	10.9545	2.0225
11	3.8934e-08	4.6571e-08	4.6564e-08	3.2185e-11	1.1962	10.9545	2.0056
(b) $\mathbf{y}_h \in S_{7h}^{9,9} \oplus S_{7h}^{9,9}$ ( $m = 7, M = 7$ )							
3	2.5648e-03	2.6756e-03	2.5800e-03	4.2495e-04	1.0432	11.0113	3.4565
5	1.5952e-04	1.7737e-04	1.6869e-04	3.8537e-05	1.1118	10.9580	2.3602
7	9.9673e-06	1.0215e-05	1.0035e-05	7.9975e-07	1.0248	10.9546	2.0901
9	6.2294e-07	6.9080e-07	6.3274e-07	2.5797e-07	1.1089	10.9545	2.0225
11	3.8934e-08	4.0932e-08	3.9140e-08	7.9608e-09	1.0513	10.9545	2.0056

Table 2: *Ex. 1.* Error, majorant (with dual and equilibrated terms), efficiency indices, and e.o.c. w.r.t. unif. ref. steps.

# ref	# d.o.f. ( $u_h$ )	# d.o.f. ( $\mathbf{y}_h$ )	$t_{\text{as}}(u_h)$	$t_{\text{as}}(\mathbf{y}_h)$	$t_{\text{sol}}(u_h)$	$t_{\text{sol}}(\mathbf{y}_h)$	$t_{e/w}(\ \nabla e\ )$	$t_{e/w}(\bar{M})$	$t_{e/w}(\bar{\eta})$
(a) $\mathbf{y}_h \in S_{3h}^{5,5} \oplus S_{3h}^{5,5}$ ( $q = 5, m = 3, M = 3$ )									
1	9	36	0.0013	0.0023	0.0001	0.0017	0.0000	0.0008	0.0006
3	36	36	0.0010	0.0025	0.0001	0.0018	0.0005	0.0025	0.0022
5	324	81	0.0094	0.0216	0.0008	0.0094	0.0087	0.0159	0.0276
7	4356	441	0.0729	0.2506	0.0439	0.0730	0.1830	0.1571	0.2858
9	66564	4761	1.2661	4.0725	3.6962	8.3926	2.5329	2.8220	4.1740
11	1052676	68121	22.4621	68.2723	211.1700	570.4293	37.8862	37.9696	65.6940
(b) $\mathbf{y}_h \in S_{7h}^{9,9} \oplus S_{7h}^{9,9}$ ( $q = 9, m = 7, M = 7$ )									
1	9	100	0.0008	0.0234	0.0001	0.0122	0.0002	0.0025	0.0004
3	36	100	0.0006	0.0167	0.0001	0.0132	0.0003	0.0038	0.0012
5	324	100	0.0089	0.0258	0.0010	0.0057	0.0048	0.0269	0.0167
7	4356	100	0.0750	0.0140	0.0401	0.0093	0.1564	0.5749	0.3073
9	66564	169	1.1129	0.1967	3.2580	0.0763	2.5923	6.2473	4.2985
11	1052676	625	17.6219	3.9372	196.0170	1.2941	35.1466	99.9845	61.1072

Table 3: *Ex. 1.* Time for assembling and solving the systems that generate  $u_h$  and  $\mathbf{y}_h$ , time for e/w evaluation of error, majorant, and residual error estimator w.r.t. unif. ref. steps.

**Example 1** First, we consider a basic example with

$$u = (1 - x_1)x_1^2(1 - x_2)x_2, \quad f = -(2(1 - 3x_1)(1 - x_2)x_2 - 2(1 - x_1)x_1^2) \quad \text{in } \Omega,$$

and homogeneous Dirichlet boundary condition (BC).

Let the primal variable be approximated by the splines of degree  $p = 2$ , i.e., the discretisation space  $S_h^{p,p}$ . For the uniform refinement (unif. ref.), we first test the idea introduced in [28] and compare two different settings for spaces approximating auxiliary dual variable  $\mathbf{y}_h \in S_{Mh}^{q,q}$ :

$$(a) \quad q = 5, \quad m = 3, \quad M = 3, \quad \text{and} \quad (b) \quad q = 9, \quad m = 7, \quad M = 7. \quad (30)$$

After performing  $N_{\text{ref}} = 11$  unif. ref. steps, we present the obtained numerical results in Tables 2–3 (where the upper and the lower parts correspond to the cases (a) and (b), respectively). The efficiency of functional error majorant is confirmed by corresponding indices, i.e.,  $I_{\text{eff}}(\bar{M}) = 1.1961$  for the case (a) and  $I_{\text{eff}}(\bar{M}) = 1.0024$  for the case (b) (see the shaded column of Table 2). The expected error order of convergence (e.o.c.)  $p = 2$  is confirmed by the last column of Table 2. The time needed for the residual-based estimate evaluation is dependent only on the approximation  $u_h$ . Since # d.o.f. ( $u_h$ ) stays the same,  $t_{e/w}(\bar{\eta})$  stays approximately the same. The time required for the evaluation of the majorant, in turn, is more complex, since it is dependent on both  $u_h$  and  $\mathbf{y}_h$ . In the case (b), it is larger than in the case (a), because majorant is evaluated on the mesh  $\mathcal{K}_h$  (the same one that is used for  $u_h$  approximation). In the same time, the degree of splines used to approximate  $y_h$  is higher ( $\mathbf{y}_h \in S_{7h}^{9,9} \oplus S_{7h}^{9,9}$ ). That is the reason we obtain an overhead in the evaluation time for the majorant. Therefore, the fact the time for evaluation of the majorant is larger than that of the residual error estimator (when higher order approximation is used) can be explained exactly by the increase of the degree of B-splines.

# ref.	$\ \nabla e\ _\Omega$	$\bar{M}$	$\bar{m}_d$	$\bar{m}_f$	$I_{\text{eff}}(\bar{M})$	$I_{\text{eff}}(\bar{\eta})$	e.o.c.
3	2.5648e-03	3.0154e-03	3.0000e-03	6.8225e-05	1.1757	11.0115	3.4566
5	1.5952e-04	1.7571e-04	1.6338e-04	5.4779e-05	1.1015	10.9580	2.3602
7	9.9672e-06	1.1959e-05	1.0675e-05	5.7051e-06	1.1998	10.9547	2.0901
9	6.2294e-07	6.4308e-07	6.3365e-07	4.1905e-08	1.0323	10.9545	2.0225
11	3.8934e-08	4.0029e-08	3.9480e-08	2.4369e-09	1.0281	10.9545	2.0056

Table 4: *Ex. 1.* Error, majorant (with dual and reliability terms), efficiency indices, and e.o.c. for  $\mathbf{y}_h \in S_{8h}^{3,3} \oplus S_{8h}^{3,3}$  w.r.t. uniform ref. steps.

# ref.	# d.o.f.( $u_h$ )	# d.o.f.( $\mathbf{y}_h$ )	$t_{\text{as}}(u_h)$	$t_{\text{as}}(\mathbf{y}_h)$	$t_{\text{sol}}(u_h)$	$t_{\text{sol}}(\mathbf{y}_h)$	$t_{e/w}(\ \nabla e\ )$	$t_{e/w}(\bar{M})$	$t_{e/w}(\bar{\eta})$
1	9	16	0.0009	0.0015	0.0000	0.0001	0.0001	0.0003	0.0003
3	36	16	0.0008	0.0005	0.0000	0.0001	0.0006	0.0007	0.0018
5	324	16	0.0081	0.0006	0.0005	0.0001	0.0184	0.0112	0.0285
7	4356	16	0.0753	0.0004	0.0173	0.0001	0.1391	0.1071	0.2534
9	66564	25	1.1899	0.0009	1.3832	0.0001	2.2776	1.6354	4.0632
11	1052676	121	19.9547	0.0114	107.0756	0.0020	36.0268	26.0721	63.6307

Table 5: *Ex. 1.* Time for assembling and solving the systems that generate  $u_h$  and  $\mathbf{y}_h$ , time for e/w evaluation of error, majorant, and residual error estimator for  $\mathbf{y}_h \in S_{8h}^{3,3} \oplus S_{8h}^{3,3}$  w.r.t. unif. ref. steps.

# ref.	$\ \nabla e\ _\Omega$	$\bar{M}$	$I_{\text{eff}}(\bar{M})$	$\underline{M}$	$I_{\text{eff}}(\underline{M})$	$\bar{M}/\underline{M}$	e.o.c.
3	2.5648e-03	3.0154e-03	1.1757	2.5648e-03	1.0000	1.1757	3.4566
5	1.5952e-04	1.7571e-04	1.1015	1.5952e-04	1.0000	1.1015	2.3602
7	9.9672e-06	1.1959e-05	1.1998	9.9672e-06	1.0000	1.1998	2.0901
9	6.2294e-07	6.4308e-07	1.0323	6.2294e-07	1.0000	1.0323	2.0225

Table 6: *Ex. 1.* Error, majorant, minorant, residual based error indicator with corresponding efficiency indices, and e.o.c. for  $\mathbf{y}_h \in S_{8h}^{3,3} \oplus S_{8h}^{3,3}$  and  $w_h \in S_{8h}^{3,3}$  w.r.t. unif. ref. steps.

When the computational costs are considered, the time spent on the reconstruction of  $\mathbf{y}_h$  (i.e.,  $t_{\text{as}}(\mathbf{y}_h) + t_{\text{sol}}(\mathbf{y}_h)$ ) is about 2 – 3 times higher than the time  $t_{\text{as}}(u_h) + t_{\text{sol}}(u_h)$  in the setting (a). However, for the case (b), the assembling time of  $\text{Div}_h$  and  $M_h$  denoted by  $t_{\text{as}}(\mathbf{y}_h)$  takes approximately 1/4-th of the assembling time for  $K_h$  denoted by  $t_{\text{as}}(u_h)$ . Similarly, solving the system (28) denoted by  $t_{\text{sol}}(\mathbf{y}_h)$  requires only 1/150-th of time spent on solving (26), i.e.,  $t_{\text{sol}}(u_h)$ .

Due to the smoothness of the exact solution in this example, we can even use splines of lower degree for the flux approximation, e.g.,  $q = 3$ , but at the same time reconstruct it on a much coarser mesh than for  $u_h$ , e.g., mesh  $M = 8$  times coarser. The resulting efficiency indices are illustrated in Table 5, and corresponding times spent on the reconstruction of  $u_h$  and  $\mathbf{y}_h$  (i.e.,  $\bar{M}(u_h, \mathbf{y}_h)$  and  $\bar{m}_d(u_h, \mathbf{y}_h)$ ) are presented in Table 4. By looking at Table 5, one can see the considerable speed-up in the time required for reconstruction of  $\mathbf{y}_h$  in comparison to  $u_h$ :

$$\frac{t_{\text{as}}(u_h)}{t_{\text{as}}(\mathbf{y}_h)} \approx \frac{19.9547}{0.0114} \approx 1750 \quad \text{and} \quad \frac{t_{\text{sol}}(u_h)}{t_{\text{sol}}(\mathbf{y}_h)} \approx \frac{107.0756}{0.0020} \approx 53538.$$

For the cases when the exact solution is not provided, the quality of the majorant can be verified by comparison of its values to the lower bound of the error. We assume that for the space approximating  $w_h \in S_h^{r,r}$ , we choose  $r = 3$ , and for the mesh  $K_{Lh}$ , the coarsening parameter is taken  $L = 8$ . To study the efficiency of the estimates, values of the majorant and minorant are compared to the error as well as to each other in Table 6. According to efficiency index  $I_{\text{eff}}(\underline{M})$ , minorant remains sharp w.r.t the increasing number of refinement steps (see column seven of Table 6). As a result, the ratio of the upper and lower bounds  $\bar{M}/\underline{M}$  is very close to one. This fact confirms that provided by  $\bar{M}$  and  $\underline{M}$  two-sided bound is guaranteed and the error of reconstructed approximation is contained inside of the interval  $[\underline{M}, \bar{M}]$ . In addition to the efficiency of the error estimates, we compare the time spent for assembling and solving systems (26), (28), and (29) in Table 6. The last rows with ratios between time spend on the  $u_h$ -approximation w.r.t.  $\mathbf{y}_h$  and  $w_h$  show that ‘expenses’ related to the approximation of latter two variables are thousand times cheaper than the time dedicated to the primal variable.

For an adaptive refinement strategy, we combine the THB-splines [29, 70, 21], which support local refinement, and functional error estimates. We use bulk marking criterion with parameter  $\theta = 0.4$ . Let us start with the following setting:  $u_h \in S_h^{2,2}$ , where  $S_h^{2,2}$  is generated by THB-splines, and  $\mathbf{y}_h \in S_{8h}^{3,3} \oplus S_{8h}^{3,3}$ , where  $S_{8h}^{3,3} \oplus S_{8h}^{3,3}$  is generated by the basis of THB-splines as well. Overall,  $N_{\text{ref}} = 11$  refinements are executed to obtain the error illustrated in Table 8. The time spent to generate  $u_h$  and  $\mathbf{y}_h$  is illustrated in Table 9. By using a mesh that is up to 8 times coarser than the one for  $u_h$ , we manage to spare computational time for reconstructing the optimal

#ref.	#d.o.f.( $u_h$ )	#d.o.f.( $\mathbf{y}_h$ )	#d.o.f.( $w_h$ )	$t_{as}(u_h)$	$t_{as}(\mathbf{y}_h)$	$t_{as}(w_h)$	$t_{sol}(u_h)$	$t_{sol}(\mathbf{y}_h)$	$t_{sol}(w_h)$
3	36	16	16	8.01e-04	4.70e-03	2.39e-03	6.20e-05	1.72e-04	3.80e-05
5	324	16	16	8.25e-03	4.95e-03	8.54e-04	1.98e-04	1.32e-04	7.00e-06
7	4356	16	16	8.73e-02	1.84e-03	2.58e-03	1.46e-02	2.08e-04	2.10e-05
9	66564	25	25	1.26e+00	1.08e-02	2.30e-03	1.38e+00	5.32e-04	1.00e-05
				547.82	: 4.69	: 1	138000	: 53.2	: 1

Table 7: *Ex. 1.* Time for solving the systems that generate  $u_h$ ,  $\mathbf{y}_h$ , and  $w_h$ , with direct and iterative methods for  $\mathbf{y}_h \in S_{8h}^{3,3} \oplus S_{8h}^{3,3}$  and  $w_h \in S_{8h}^{3,3}$  w.r.t. unif. ref. steps.

# ref.	$\ \nabla e\ _\Omega$	$\bar{M}$	$\bar{m}_d^2$	$\bar{m}_{eq}^2$	$I_{eff}(\bar{M})$	$I_{eff}(\bar{\eta})$	e.o.c.
3	7.9113e-03	8.9838e-03	8.1878e-03	3.5362e-03	1.1356	8.7164	0.9252
5	5.5188e-04	7.5068e-04	7.3580e-04	6.6131e-05	1.3602	9.9802	2.9781
7	4.8373e-05	6.1113e-05	5.9155e-05	8.7003e-06	1.2634	10.0270	2.4156
9	6.1176e-06	8.6725e-06	8.4757e-06	8.7451e-07	1.4176	10.3944	1.6446
11	6.1657e-07	6.3268e-07	6.2654e-07	2.7268e-08	1.0261	10.7801	2.5543

Table 8: *Ex. 1.* Error, majorant (with dual and reliability terms), efficiency indices, and e.o.c. w.r.t. adaptive ref. steps with the marking  $\mathbb{M}_{BULK}(0.2)$ .

#ref.	#d.o.f.( $u_h$ )	#d.o.f.( $\mathbf{y}_h$ )	$t_{as}(u_h)$	$t_{as}(\mathbf{y}_h)$	$t_{sol}(u_h)$	$t_{sol}(\mathbf{y}_h)$	$t_{e/w}(\ \nabla e\ )$	$t_{e/w}(\bar{M})$	$t_{e/w}(\bar{\eta})$
3	36	16	0.0055	0.0021	0.0001	0.0002	0.0032	0.0146	0.0170
5	305	16	0.0839	0.0023	0.0008	0.0002	0.1223	0.1920	0.2382
7	3224	16	1.4683	0.0035	0.0581	0.0002	1.4490	2.8517	2.8234
9	38276	16	27.1005	0.0021	1.9923	0.0002	22.0243	30.7559	38.1258
11	396360	49	3153.3647	0.0495	73.2963	0.0017	218.8799	328.0449	410.5585

Table 9: *Ex. 1.* Time for assembling and solving the systems that generate  $u_h$  and  $\mathbf{y}_h$ , time for e/w evaluation of error, majorant, and residual error estimator w.r.t. adaptive ref. steps with the marking  $\mathbb{M}_{BULK}(0.2)$ .

# ref.	$\ \nabla e\ _\Omega$	$\bar{M}$	$\bar{m}_d^2$	$\bar{m}_{eq}^2$	$I_{eff}(\bar{M})$	$I_{eff}(\bar{\eta})$	e.o.c.
2	5.5286e-02	6.3291e-02	5.7322e-02	2.6518e-02	1.1448	10.3894	3.9940
4	3.2077e-03	4.0140e-03	3.4919e-03	2.3195e-03	1.2514	10.9176	2.3839
5	7.9894e-04	1.4534e-03	1.4273e-03	1.1597e-04	1.8191	10.9451	2.1856
6	1.9955e-04	1.2390e-03	1.1931e-03	2.0405e-04	6.2091	10.9521	2.0914
8	1.2468e-05	9.8611e-05	3.7673e-05	2.7074e-04	7.9091	10.9543	2.0226
10	7.7924e-07	8.4668e-07	7.7970e-07	2.9758e-07	1.0865	10.9544	2.0056

Table 10: *Ex. 2,*  $k_1 = k_2 = 1$ . Error, majorant (with dual and reliability terms), efficiency indices, and e.o.c. w.r.t. unif. ref. steps.

$\mathbf{y}_h$  and speed up the overall reconstruction of majorant. In the current configuration, we obtain the following ratios:

$$\frac{t_{as}(u_h)}{t_{as}(\mathbf{y}_h)} \approx \frac{3153.3647}{0.0495} \approx 63704 \quad \text{and} \quad \frac{t_{sol}(u_h)}{t_{sol}(\mathbf{y}_h)} \approx \frac{73.2963}{0.0017} \approx 43115.$$

The comparison of meshes obtained while refining with different parameters can be found on Figure 5, i.e.,  $\theta = 0.4$  (left column) and  $\theta = 0.2$  (right column). It is obvious from the plots that the smaller bulk parameter  $\theta$  is, the higher the percentage of refined elements in the mesh is.

**Example 2** Next, we consider an example with the exact solution, such that its gradient growth is controlled by the parameters. This way, we can study properties of the majorant on the subdomains of  $\Omega$ , where  $u_h$  has fast-growing gradients. Namely, we let  $\Omega$  be a unit square, and let the exact solution and RHS be chosen as follows:

$$\begin{aligned} u &= \sin(k_1 \pi x_1) \sin(k_2 \pi x_2) && \text{in } \Omega, \\ f &= (k_1^2 + k_2^2) \pi^2 \sin(k_1 \pi x_1) \sin(k_2 \pi x_2) && \text{in } \Omega, \\ u_D &= 0 && \text{on } \Gamma. \end{aligned}$$

First, let  $k_1 = k_2 = 1$ . For such parameters, the exact solution is illustrated in Figure 6a. The function  $u_h$  is approximated by  $S_h^{2,2}$ , whereas  $\mathbf{y}_h \in S_{6h}^{5,5} \oplus S_{6h}^{5,5}$ , and  $N_{ref} = 11$  unif. ref. steps are considered. The resulting performance of majorant is presented in Table 10. At the same time, the computational effort spent

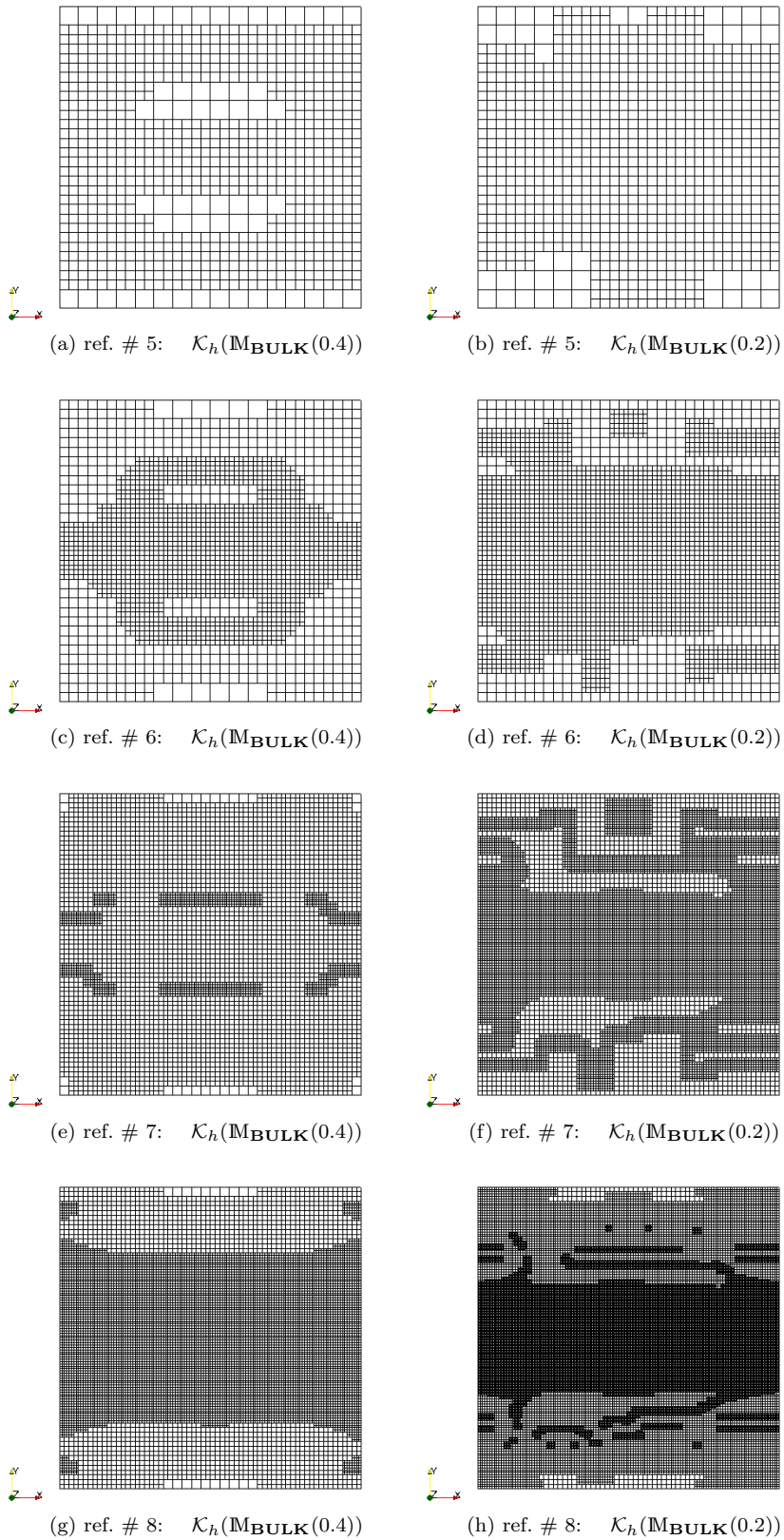


Figure 5: *Ex. 1.* Evolution of adaptive meshes obtained with the marking criteria  $\mathcal{M}_{\text{BULK}}(0.4)$  and  $\mathcal{M}_{\text{BULK}}(0.2)$  w.r.t. adaptive ref. steps.

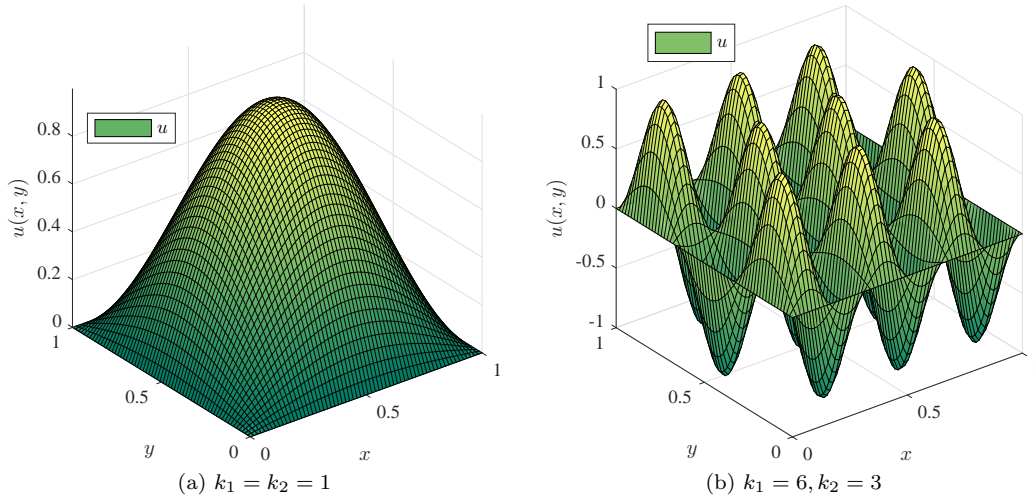


Figure 6: *Ex. 2.* Exact solution  $u = \sin(k_1 \pi x_1) \sin(k_2 \pi x_2)$ .

# ref.	# d.o.f.( $u_h$ )	# d.o.f.( $\mathbf{y}_h$ )	$t_{as}(u_h)$	$t_{as}(\mathbf{y}_h)$	$t_{sol,dir}(u_h)$	$t_{sol,dir}(\mathbf{y}_h)$	$t_{sol,iter}(u_h)$	$t_{sol,iter}(\mathbf{y}_h)$
2	36	36	0.0007	0.0013	0.0001	0.0014	0.0000	0.0010
4	324	36	0.0091	0.0016	0.0013	0.0010	0.0001	0.0007
5	1156	36	0.0289	0.0015	0.0057	0.0008	0.0598	0.1015
6	4356	36	0.0723	0.0017	0.0342	0.0007	0.0067	0.0003
8	66564	81	1.5561	0.0141	3.1404	0.0036	0.6299	0.0045
10	1052676	441	20.2540	0.2224	166.5165	0.1367	33.6298	0.1121

Table 11: *Ex. 2,*  $k_1 = k_2 = 1$ . Time for assembling and solving the systems that generate  $u_h$  and  $\mathbf{y}_h$  (with direct and iterative solvers).

# ref.	$\ \nabla e\ _{\Omega}$	$\bar{M}$	$I_{\text{eff}}(\bar{M})$	$\underline{M}$	$I_{\text{eff}}(\underline{M})$	$\bar{M}/\underline{M}$	e.o.c.
3	5.5285e-02	5.7554e-02	1.0411	5.5115e-02	0.9969	1.0443	3.9940
4	1.3024e-02	1.6545e-02	1.2704	1.3012e-02	0.9991	1.2715	2.8302
6	1.6936e-03	2.2063e-03	1.3027	1.6885e-03	0.9970	1.3067	1.6060
7	4.5250e-04	1.2058e-03	2.6648	4.3221e-04	0.9552	2.7898	2.1530
8	1.6513e-04	2.2145e-04	1.3411	1.6487e-04	0.9984	1.3432	1.9801
9	5.4927e-05	1.2373e-04	2.2527	5.4114e-05	0.9852	2.2865	3.8077

Table 12: *Ex. 2.* Error, majorant, minorant, residual based error indicator with corresponding efficiency indices, and e.o.c. for  $\mathbf{y}_h \in S_{6h}^{6,6} \oplus S_{6h}^{6,6}$  and  $w_h \in S_{6h}^{7,7}$  w.r.t. adaptive ref. steps.

on  $\mathbf{y}_h$ -reconstruction is several times lower than for  $u_h$ , i.e.,

$$\frac{t_{as}(u_h)}{t_{as}(\mathbf{y}_h)} \approx \frac{20.2540}{0.2224} \approx 91 \quad \text{and} \quad \frac{t_{sol}(u_h)}{t_{sol}(\mathbf{y}_h)} \approx \frac{166.5165}{0.1367} \approx 1218,$$

which can be observed from Table 11.

Let us assume again that the exact solution is not given a priori. Then, reconstruction of the minorant can help to evaluate the reliability of the error majorant. The performance of the latter one is illustrated in Table 12, whereas Table 13 provides the comparison of the time one spends on the reconstruction of  $u_h$  as well as  $\mathbf{y}_h$  and  $w_h$ . It is easy to observe from the column providing the ratios  $\bar{M}/\underline{M}$  that values of  $\bar{M}$  are quite reliable and efficient. Moreover, Table 13 confirms that the expenses on the reconstruction of both  $\bar{M}$  and  $\underline{M}$  are rather modest in comparison to the expenses on the primal variable.

Let us consider now a more complicated case with  $k_1 = 6$  and  $k_2 = 3$  (see Figure 6b). For an efficient flux reconstruction, we apply the same strategy as discussed in *Ex. 1*, i.e., we increase the degree of B-splines used for the space approximating  $\mathbf{y}_h$ , but at the same time, we use  $M = 8$  times coarser mesh, i.e.,  $S_{8h}^{9,9} \oplus S_{8h}^{9,9}$ . First, we analyse the results obtained by global refinement; they are presented in Tables 14 and 15. We consider  $N_{\text{ref}} = 8$  unif. ref. steps (starting from a rather fine initial mesh generated by  $N_{\text{ref},0} = 4$  initial ref. steps of original geometry and the basis assigned for it). In column six of Table 14, one can see that  $I_{\text{eff}}$  takes values up to 6.2091 but decreases back to 1.0865 once we start refining the basis for the variable  $\mathbf{y}_h$  as well. In particular,

#ref.	#d.o.f.( $u_h$ )	#d.o.f.( $\mathbf{y}_h$ )	#d.o.f.( $w_h$ )	$t_{as}(u_h)$	$t_{as}(\mathbf{y}_h)$	$t_{as}(w_h)$	$t_{sol}(u_h)$	$t_{sol}(\mathbf{y}_h)$	$t_{sol}(w_h)$
1	9	49	64	2.14e-03	3.80e-02	2.88e-02	3.60e-05	1.11e-03	1.70e-05
3	36	49	64	8.72e-03	3.96e-02	2.61e-02	5.50e-05	2.23e-03	1.29e-04
4	100	49	64	2.89e-02	3.10e-02	2.53e-02	1.40e-05	2.50e-03	3.60e-05
6	952	49	64	5.65e-01	3.56e-02	2.25e-02	2.74e-03	2.03e-03	5.80e-05
7	3244	49	64	1.34e+00	1.93e-02	2.02e-02	8.11e-03	1.21e-03	1.02e-04
8	8980	64	81	5.68e+00	1.19e-01	6.92e-02	1.01e-01	3.46e-03	7.00e-05
9	16009	64	81	5.88e+00	8.24e-02	6.07e-02	2.34e-01	2.78e-03	9.70e-05
				96.86	: 1.35	: 1	2412.37	: 28.66	: 1

Table 13: *Ex. 2.* Time for solving the systems that generate  $u_h$ ,  $\mathbf{y}_h$ , and  $w_h$ , with direct and iterative methods for  $\mathbf{y}_h \in S_{6h}^{6,6} \oplus S_{6h}^{6,6}$  and  $w_h \in S_{6h}^{7,7}$  w.r.t. adaptive ref. steps.

# ref.	$\ \nabla e\ _\Omega$	$\bar{M}$	$\bar{m}_d^2$	$\bar{m}_{eq}^2$	$I_{eff}(\bar{M})$	$I_{eff}(\bar{\eta})$	e.o.c.
3	3.1030e-02	3.1818e-02	3.1057e-02	3.3805e-03	1.0254	10.8671	2.1371
5	1.9203e-03	1.9909e-03	1.9303e-03	2.6939e-04	1.0367	10.9490	2.0254
7	1.1995e-04	1.8194e-04	1.2028e-04	2.7397e-04	1.5168	10.9541	2.0058

Table 14: *Ex. 2,*  $k_1 = 6, k_2 = 3$ . Error, majorant (with dual and reliability terms), efficiency indices, and e.o.c. w.r.t. unif. ref. steps.

at the refinements steps 5 and 6, the initial mesh of 36 d.o.f. or  $\mathbf{y}_h$  becomes relatively coarse in comparison to the basis for  $u_h$  and must be refined in order to obtain efficient values of  $\bar{M}$ . Concerning the time spent on assembling and solving the systems in (26) and (28), we obtain the following ratios taken from Table 15, namely,

$$\frac{t_{as}(u_h)}{t_{as}(\mathbf{y}_h)} \approx \frac{17.3623}{3.2302} \approx 2 \quad \text{and} \quad \frac{t_{sol}(u_h)}{t_{sol}(\mathbf{y}_h)} \approx \frac{144.7056}{1.3482} \approx 107.$$

In the case of adaptive refinement, we also use the space  $S_{7h}^{9,9} \oplus S_{7h}^{9,9}$  generated by THB-splines. Let the bulk threshold be defined by parameter  $\theta = 0.4$ , which causes the refinement of approximately 60% of all elements for the primal variable  $u_h$ . The obtained numerical results are presented in Tables 16–17.

# ref.	# d.o.f.( $u_h$ )	# d.o.f.( $\mathbf{y}_h$ )	$t_{as}(u_h)$	$t_{as}(\mathbf{y}_h)$	$t_{sol}(u_h)$	$t_{sol}(\mathbf{y}_h)$	$t_{e/w}(\ \nabla e\ )$	$t_{e/w}(\bar{M})$	$t_{e/w}(\bar{\eta})$
1	324	625	0.0053	2.9646	0.0007	0.2622	0.0047	0.1177	0.0158
3	4356	625	0.0831	3.4472	0.0396	0.6094	0.2142	0.4602	0.3388
5	66564	625	1.1135	2.9721	2.3809	1.5243	2.4025	6.4769	3.9421
7	1052676	625	17.3623	3.2302	144.7056	1.3482	45.4342	102.9160	71.1602

Table 15: *Ex. 2,*  $k_1 = 6, k_2 = 3$ . Time for assembling and solving the systems that generate  $u_h$  and  $\mathbf{y}_h$  as well as the time spent on e/w evaluation of error, majorant, and residual error estimator w.r.t. unif. ref. steps.

Let us compare the performance of majorant in the uniform and adaptive refinement strategies. Due to the implementation of THB-splines evaluation on G+Smo [38], the assembling of matrices both for  $\mathbf{y}_h$  and  $u_h$  is slower w.r.t. B-splines (compare the third and fourth columns of Table 17 to the third and fourth columns of Table 15). For d.o.f.( $u_h$ )  $\approx 4000$ , in the first case we spend  $t_{as}(u_h) = 0.0813$  secs (second row is highlighted with grey background in Table 15) in comparison to  $t_{as}(u_h) = 3.1285$  secs for the THB-splines (row with grey background in Table 17), which is about 45 times slower. Moreover, these ratios grow as d.o.f.( $u_h$ ) increases. For the auxiliary variable  $\mathbf{y}_h$ , the assembling time for THB-splines is 4–5 times slower than when using B-splines. A similar increase in time can be observed for the element-wise evaluation of the error, majorant, and residual error estimator illustrated in the last three columns of Table 17 (in comparison to Table 15). This slowdown can be explained by a bottleneck of G+Smo library when the evaluation of THB-splines is concerned.

Analogously to the previous example, we demonstrate the evaluation of adaptive meshes for different marking criteria, i.e., marking  $\mathbf{M}_{BULK}(0.4)$  (left column of Figure 7) and  $\mathbf{M}_{BULK}(0.6)$  (right column of Figure 7). It resembles the patterns obtained in [28, Example 1], however, in the current case, due to the local structure of THB-splines, many superfluous d.o.f. are eliminated.

**Example 3** Next, we consider an example with a sharp local jump in the exact solution. Let  $\Omega := (0, 2) \times (0, 1)$ ,

$$u = (x_1^2 - 2x_1)(x_2^2 - x_2)e^{-100|(x_1, x_2) - (1.4, 0.95)|} \quad \text{in } \Omega,$$

where the jump is located in the point  $(x_1, x_2) = (1.4, 0.95)$  (see Figure 8),  $f$  is calculated by substituting  $u$  into (25), and the Dirichlet BCs are homogenous. First, we run the test with the global ref. strategy. The obtained

$N_{\text{ref}}$	$\ \nabla e\ _{\Omega}$	$\bar{M}$	$\bar{m}_d^2$	$\bar{m}_{\text{eq}}^2$	$I_{\text{eff}}(\bar{M})$	$I_{\text{eff}}(\bar{\eta})$	e.o.c.
3	4.2892e-02	4.3740e-02	4.2910e-02	3.6902e-03	1.0198	9.6688	2.1266
5	5.3723e-03	5.5714e-03	5.4777e-03	4.1637e-04	1.0371	9.9389	1.8082
7	6.4564e-04	7.2116e-04	6.5719e-04	2.8420e-04	1.1170	10.5034	2.3521

Table 16: *Ex. 2*,  $k_1 = 6, k_2 = 3$ . Error, majorant (with dual and reliability terms), efficiency indices w.r.t. adaptive ref. steps.

# ref.	# d.o.f. ( $u_h$ )	# d.o.f. ( $\mathbf{y}_h$ )	$t_{\text{as}}(u_h)$	$t_{\text{as}}(\mathbf{y}_h)$	$t_{\text{sol}}(u_h)$	$t_{\text{sol}}(\mathbf{y}_h)$	$t_{e/w}(\ \nabla e\ )$	$t_{e/w}(\bar{M})$	$t_{e/w}(\bar{\eta})$
1	324	625	0.1125	23.3092	0.0010	0.2418	0.0918	7.0919	0.1938
3	3468	625	1.2291	22.0679	0.0313	0.6313	1.5198	12.0444	2.9476
5	31640	625	44.5650	22.1864	0.9953	1.2794	18.0067	107.7677	32.6181
7	205060	625	1135.8096	21.3158	17.4630	1.3050	105.0698	583.0759	190.6939

Table 17: *Ex. 2*,  $k_1 = 6, k_2 = 3$ . Time for assembling and solving the systems generating d.o.f. of  $u_h$  and  $\mathbf{y}_h$  as well as the time spent on e/w evaluation of error, majorant, and residual error estimator w.r.t. adaptive ref. steps.

# ref.	$\ \nabla e\ _{\Omega}$	$\bar{M}$	$\bar{m}_d^2$	$\bar{m}_{\text{eq}}^2$	$I_{\text{eff}}(\bar{M})$	$I_{\text{eff}}(\bar{\eta})$	e.o.c.
2	5.5665e-03	1.7635e-01	5.6126e-02	4.2226e-01	31.6798	8.5283	2.9617
4	2.6655e-04	1.1913e-02	4.0094e-03	2.7762e-02	44.6942	10.6943	2.1266
6	1.6374e-05	3.0360e-05	1.7856e-05	4.3919e-05	1.8541	10.8469	2.0163
8	1.0223e-06	1.1654e-06	1.1146e-06	1.7861e-07	1.1400	10.8565	2.0031

Table 18: *Ex. 3*. Error, majorant (with dual and reliability terms), efficiency indices, and e.o.c. w.r.t. unif. ref. steps.

# ref.	# d.o.f. ( $u_h$ )	# d.o.f. ( $\mathbf{y}_h$ )	$t_{\text{as}}(u_h)$	$t_{\text{as}}(\mathbf{y}_h)$	$t_{\text{sol}}(u_h)$	$t_{\text{sol}}(\mathbf{y}_h)$	$t_{e/w}(\ \nabla e\ )$	$t_{e/w}(\bar{M})$	$t_{e/w}(\bar{\eta})$
2	1156	400	0.0299	0.1359	0.0058	0.0254	0.0705	0.0665	0.1066
4	16900	1296	0.5347	0.5352	0.4255	0.1728	0.9429	0.6846	1.4733
6	264196	17424	7.3424	7.9156	23.5576	16.7765	14.1433	10.1504	22.3347
8	4202500	266256	107.9652	121.7985	1516.5229	970.6061	238.5717	155.4827	370.6186

Table 19: *Ex. 3*. Time for assembling and solving the systems that generate  $u_h$  and  $\mathbf{y}_h$  as well as the time spent on e/w evaluation of error, majorant, and residual error estimator w.r.t. unif. ref. steps.

results are summarised in Tables 18–19. Several systematically performed tests demonstrated that in order to perform a reliable estimation of the error in  $u_h \in S_h^{2,2}$ , it is optimal to take  $\mathbf{y}_h \in S_{3h}^{4,4} \oplus S_h^{4,4}$ , i.e., we obtain efficient error bounds with the minimal computation effort spent on assembling and solving (28).

Still, the most interesting test-case is the one that checks the performance of the majorant for the adaptive refinement. A series of tests showed that the optimal setting (in terms of quality of the error bounds and computational time spent on its reconstruction) is the approximation of  $\mathbf{y}_h$  with THB-basis functions of the degree 4, i.e.,  $\mathbf{y}_h \in S_h^{4,4} \oplus S_h^{4,4}$ . At the same time, we consider the same mesh  $\mathcal{K}_h$  that is used for approximation of  $u_h$ . The obtained decrease of error and majorant with the marking criteria  $\mathbf{M}_{\text{BULK}}(0.4)$  and  $\mathbf{M}_{\text{BULK}}(0.6)$  is illustrated in Table 20, the corresponding time expenses are summarised in Table 21. The most efficient error decrease is obtained for the bulk parameter  $\theta = 0.4$ , which can be detected from Figure 9.

Figure 10 presents the evolution of physical meshes obtained during the refinement steps with different marking criteria  $\mathbf{M}_{\text{BULK}}(0.4)$  and  $\mathbf{M}_{\text{BULK}}(0.2)$ . Again, it is easy to observe from the graphics that the percentage of the refined elements on the right is higher than the percentage of such elements on the left.

When the exact solution contains large local changes in the gradient (such as the one in the current example), the assembling and solving the system (28) becomes computationally heavier than respective procedures for (26). This can be explained by the size of the generated optimal system (28) providing the reconstruction of vector-valued  $\mathbf{y}_h$ . This drawback can be possibly eliminated by introducing multi-threading techniques (e.g., OpenMP, MPI) into the implementation of THB-splines. However, this matter stays beyond the focus of current paper and will be addressed in the upcoming technical report.

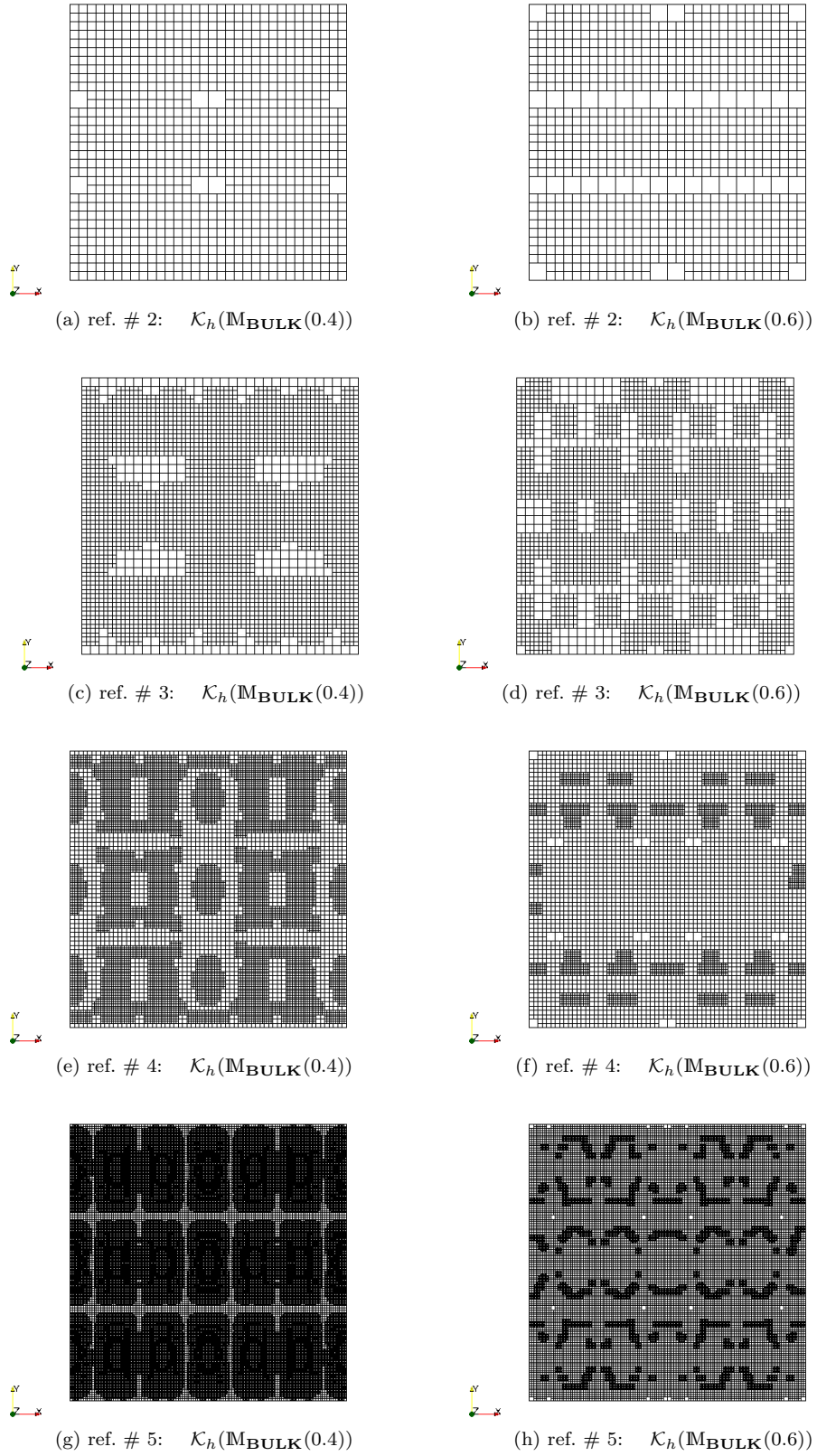


Figure 7: *Ex. 2*,  $k_1 = 6, k_2 = 3$ . Evolution of adaptive meshes obtained with the marking criteria  $\mathbf{M}_{\text{BULK}}(0.4)$  (left) and  $\mathbf{M}_{\text{BULK}}(0.6)$  (right) w.r.t. adaptive ref. steps.

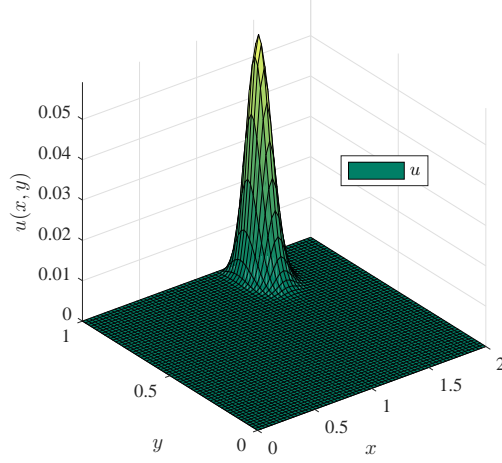


Figure 8: *Ex. 3.* Exact solution  $u = (x_1^2 - 2x_1)(x_2^2 - x_2)e^{-100|(x_1, x_2) - (1.4, 0.95)|}$ .

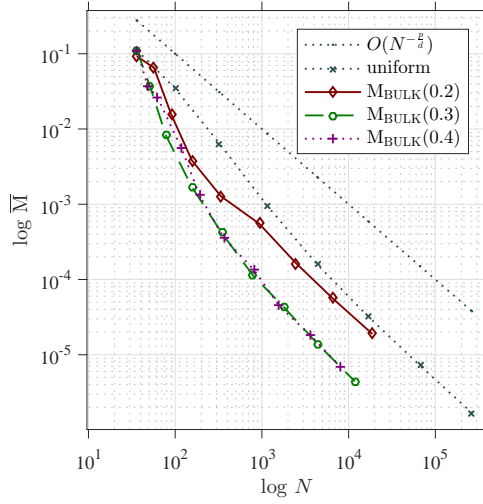


Figure 9: Convergence of the majorant for different marking criteria.

# ref.	$\ \nabla e\ _\Omega$	$\bar{M}$	$\bar{m}_d^2$	$\bar{m}_{eq}^2$	$I_{\text{eff}}(\bar{M})$	$I_{\text{eff}}(\bar{\eta})$	e.o.c.
(a) $\theta = 0.4$							
2	4.0502e-02	2.8670e-01	1.0725e-01	6.3030e-01	7.0786	5.5395	3.8159
4	5.2223e-03	3.7058e-02	1.5518e-02	7.5657e-02	7.0960	8.9835	4.7759
6	8.7993e-04	2.1154e-03	9.8705e-04	3.9631e-03	2.4040	8.6122	3.3554
8	1.1156e-04	1.9665e-04	1.1451e-04	2.8852e-04	1.7627	9.5564	2.8809
(b) $\theta = 0.2$							
2	3.6612e-02	2.0753e-01	8.3292e-02	4.3637e-01	5.6683	5.7646	3.0397
4	1.3527e-03	4.0090e-03	1.6115e-03	8.4210e-03	2.9637	9.3503	5.0006
6	1.5416e-04	3.1033e-04	1.6976e-04	4.9375e-04	2.0130	10.0080	2.0152
8	1.7351e-05	2.2095e-05	1.7587e-05	1.5832e-05	1.2734	10.4611	2.1194

Table 20: *Ex. 3.* Error, majorant (with dual and reliability terms), efficiency indices, error, e.o.c. w.r.t. adaptive ref. steps.

**Example 4** One of the classical benchmark examples (containing a singularity in the exact solution) is the problem with a  $L$ -shaped domain  $\Omega := (-1, 1) \times (-1, 1) \setminus [0, 1) \times [0, 1)$ . The Dirichlet BC are defined on  $\Gamma$  by the load  $u_D = r^{1/3} \sin(\theta)$ , where

$$r = (x_1^2 + x_2^2) \quad \text{and} \quad \theta = \begin{cases} \frac{1}{3}(2 \operatorname{atan2}(x_2, x_1) - \pi), & x_2 > 0, \\ \frac{1}{3}(2 \operatorname{atan2}(x_2, x_1) + 3\pi), & x_2 \leq 0. \end{cases}$$

# ref.	# d.o.f.( $u_h$ )	# d.o.f.( $\mathbf{y}_h$ )	$t_{\text{as}}(u_h)$	$t_{\text{as}}(\mathbf{y}_h)$	$t_{\text{sol}}(u_h)$	$t_{\text{sol}}(\mathbf{y}_h)$	$t_{e/w}(\ \nabla e\ )$	$t_{e/w}(\overline{M})$	$t_{e/w}(\overline{\eta})$
(a) $\theta = 0.4$									
2	124	145	0.0547	0.4156	0.0002	0.0025	0.0532	0.1738	0.1418
4	243	245	0.2481	2.6372	0.0008	0.0063	0.3529	0.9892	0.9102
6	736	633	0.7903	10.7018	0.0052	0.0393	0.9605	3.5833	2.2969
8	2460	2231	2.3106	33.6222	0.0349	0.4035	2.9163	11.5602	4.4633
(b) $\theta = 0.2$									
2	140	160	0.0449	0.3684	0.0002	0.0028	0.0651	0.1682	0.1111
4	366	366	0.2435	2.7071	0.0015	0.0124	0.3104	1.0138	0.5248
6	2043	1883	1.8328	25.3480	0.0246	0.3000	2.0493	8.0682	3.4391
8	15373	13974	17.4622	264.3344	0.4683	8.7014	15.9445	58.1277	25.9898

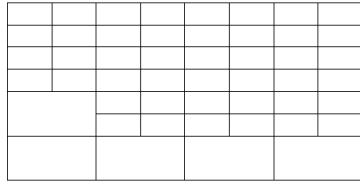
Table 21: *Ex. 3.* Time for assembling and solving the systems generating d.o.f. of  $u_h$  and  $\mathbf{y}_h$  as well as the time spent on e/w evaluation of error, majorant, and residual error estimator w.r.t. adaptive ref. steps.

The corresponding exact solution  $u = u_D$  has the singularity in the point  $(r, \theta) = (0, 0)$  (see also Figure 11a).

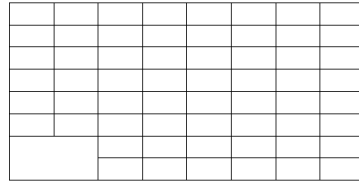
The initial geometry data and the mesh are defined by Greville's points with double control points in the corners marked with red circled markers in Figure 11b, and considered knots-vectors  $\kappa = \{0, 0, 0, 0.25, 0.5, 0.75, 1, 1, 1\}$  and  $s = \{0, 0, 0, 0.5, 1, 1, 1\}$ . Due to the doubled control points in the corners of the L-shape domain, only the re-entrant corner and its counterpart on the other side are singular (instead of the whole diagonal), i.e., the Jacobian of the geometry map in these two points is not regular. Since no integration points are placed at these corners, computational evaluation of the integrals make sense. The downside of such a setting is that with the increase of refinement steps the cells near these corners become rather thin and loose shape-regularity. In addition, since on the functional level the requirements on the regularity of  $\mathbf{y}$  is not fulfilled, the global error estimate is not reliable and has rather heuristic character, therefore, we only consider its performance from error indication point of view.

For these settings, the performance of the error majorant is compared to the performance of the residual error indicator in Table 22, where the first one is constructed with the help of fluxes  $\mathbf{y}_h \in S_h^{3,3} \oplus S_h^{3,3}$ . By increasing the degree of splines that approximate  $\mathbf{y}_h$ , one could reconstruct a sharper indicator from  $\overline{M}$ . Whereas the residual error estimate (dependent only on  $u_h$  and local  $h_K$ ) always stays on the same 'accuracy level', i.e.,  $I_{\text{eff}}(\overline{\eta}) \approx 183.3358$ . So the advantage of using the error majorant instead of residual-based error estimates is rather obvious for such kind of problems. However, the time required for reconstruction of  $\overline{M}$ , increases as well (see Table 23). Hence, the selection of space for the dual variable  $\mathbf{y}_h$  is always dependent on the smoothness of the exact solution (or RHS) and on the allocated time for the a posteriori error estimates control.

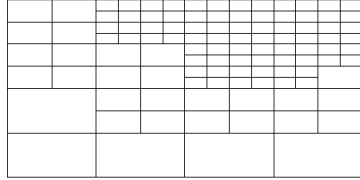
In Figure 13, we illustrate the evolution of the adaptive meshes discretising parametric domain  $\widehat{\Omega}$  (left) and corresponding to them meshes discretising physical domain  $\Omega$  (right). From presented graphics, one can see that the refinement is localised in the area close to the singularity point and no superfluous refinement is performed. We also perform the test, where, starting with the same initial mesh Figure 11b, we compare  $\mathcal{K}_h$  generated by the refinement based on the majorant (error indicator  $\overline{m}_{d,K}^2$ ) and by the refinement based on true error distribution  $\|\nabla e\|_K^2$  (with bulk parameter for the marking chosen to be  $\theta = 0.2$ ). These meshes are illustrated in Figure 12, and it is obvious that the majorant provides an adequate strategy for the adaptive refinement. The efficiency of the studied error bounds is also confirmed by comparing of majorant decrease for different marking criteria with respect to the # d.o.f.( $u_h$ ). In particular, Figure 14 shows that using majorant in combination with different markers does not only improve e.o.c. (in comparison to the one provided by the uniform refinement) but provides an even better one than  $p = 2$ . In the limit with  $h \rightarrow 0$ , the e.o.c. for the refinement strategy using any marking criteria is similar. However, on the initial refinement steps GARU (greatest appearing residual utilisation) marker locate those elements, where the error at least 90% of the highest error (over all the elements discretising the domain). For the considered L-shape domain, the maximum error is very high on first refinement steps and is mainly localised in the area close to the singular corner. Taking that into account, GARU90% selects small number of  $K \in \mathcal{K}_h$  with very high errors. After the refinement, new elements contribute with smaller values into the absolute maximum error and eventually e.o.c. becomes similar to the other marking strategies. PUCA10% marking criterion, in turn, always refines 90% of total number of the elements (such that the one with the highest errors come first). Such a strategy is not connected to the values of the distributed error. Therefore, the error decay using PUCA10% is rather latent w.r.t to the number of refinements.



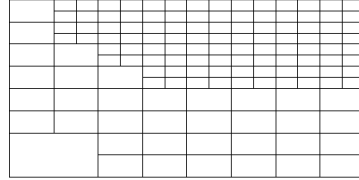
(a) ref. # 3:  $\mathcal{K}_h(\mathbf{M}_{\text{BULK}}(0.4))$



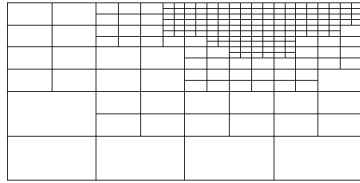
(b) ref. # 3:  $\mathcal{K}_h(\mathbf{M}_{\text{BULK}}(0.2))$



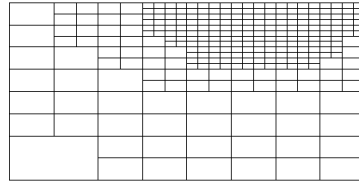
(c) ref. # 4:  $\mathcal{K}_h(\mathbf{M}_{\text{BULK}}(0.4))$



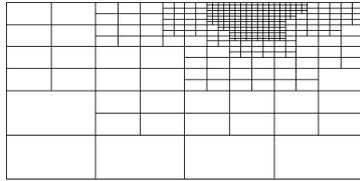
(d) ref. # 4:  $\mathcal{K}_h(\mathbf{M}_{\text{BULK}}(0.2))$



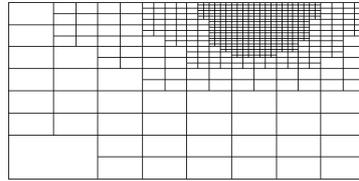
(e) ref. # 5:  $\mathcal{K}_h(\mathbf{M}_{\text{BULK}}(0.4))$



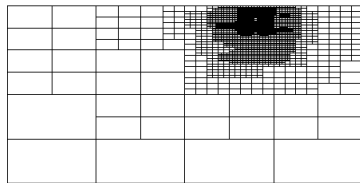
(f) ref. # 5:  $\mathcal{K}_h(\mathbf{M}_{\text{BULK}}(0.2))$



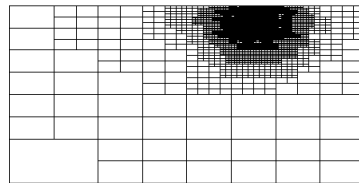
(g) ref. #6:  $\mathcal{K}_h(\mathbf{M}_{\text{BULK}}(0.4))$



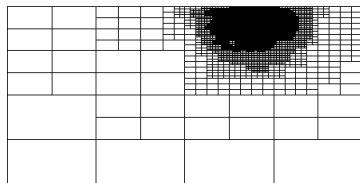
(h) ref. # 6:  $\mathcal{K}_h(\mathbf{M}_{\text{BULK}}(0.2))$



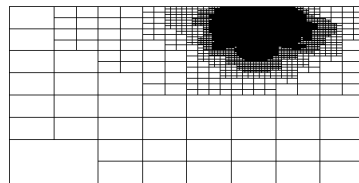
(i) ref. # 8:  $\mathcal{K}_h(\mathbf{M}_{\text{BULK}}(0.4))$



(j) ref. # 8:  $\mathcal{K}_h(\mathbf{M}_{\text{BULK}}(0.2))$



(k) ref. # 9:  $\mathcal{K}_h(\mathbf{M}_{\text{BULK}}(0.4))$



(l) ref. # 9:  $\mathcal{K}_h(\mathbf{M}_{\text{BULK}}(0.2))$

Figure 10: *Ex. 3.* Adaptive meshes obtained for the bulk parameters  $\theta = 0.4$  (left) and  $\theta = 0.2$  (right).

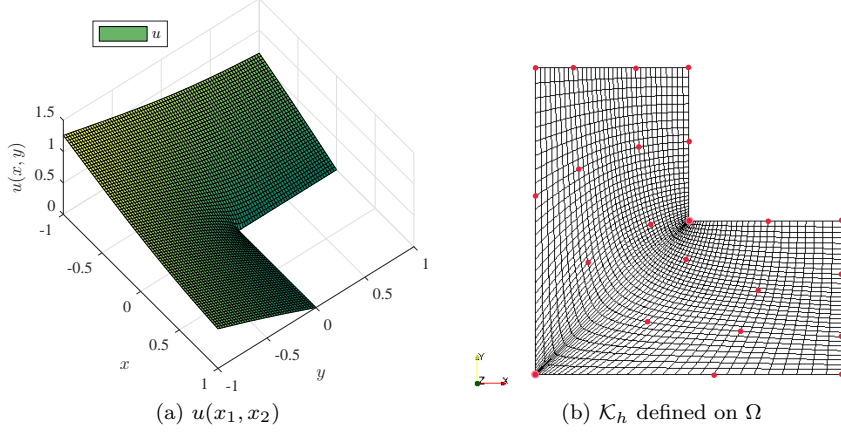


Figure 11: *Ex. 4.* (a) Exact solution  $u = r^{1/3} \sin(\theta)$ . (b) Initial geometry data with Greville's points with double control points at the corners and a corresponding mesh generated with  $C^1$ -continuous geometrical mapping.

# ref.	$\ \nabla e\ _\Omega$	$\bar{M}$	$\bar{m}_d^2$	$\bar{m}_{eq}^2$	$I_{\text{eff}}(\bar{M})$	$I_{\text{eff}}(\bar{\eta})$	e.o.c.
2	1.3359e-02	3.6140e-02	2.7595e-02	1.8983e-02	2.7053	42.6770	5.5339
3	8.7388e-03	2.3661e-02	1.8061e-02	1.2442e-02	2.7076	55.7909	6.0339
4	5.7148e-03	1.5862e-02	1.1998e-02	8.5837e-03	2.7755	74.0819	4.5481
5	3.7337e-03	1.0751e-02	8.0370e-03	6.0286e-03	2.8794	99.4303	2.4711
6	2.4386e-03	7.3896e-03	5.4326e-03	4.3474e-03	3.0303	134.3125	1.7454
7	1.5774e-03	4.8596e-03	3.6979e-03	2.5806e-03	3.0807	183.3358	1.3410

Table 22: *Ex. 4.* Error, majorant (with dual and reliability terms), efficiency indices, error, e.o.c. w.r.t. adaptive ref. steps,  $\mathbf{y}_h \in S_h^{3,3} \oplus S_h^{3,3}$ .

# ref.	# d.o.f. ( $u_h$ )	# d.o.f. ( $\mathbf{y}_h$ )	$t_{\text{as}}(u_h)$	$t_{\text{as}}(\mathbf{y}_h)$	$t_{\text{sol}}(u_h)$	$t_{\text{sol}}(\mathbf{y}_h)$	$t_{e/w}(\ \nabla e\ )$	$t_{e/w}(\bar{M})$	$t_{e/w}(\bar{\eta})$
1	612	760	0.2051	1.6904	0.0001	0.0437	0.3510	1.2626	0.6734
3	823	971	0.2290	2.1511	0.0013	0.0559	0.3223	1.8207	0.6083
5	1400	1543	0.5463	7.1518	0.0069	0.1361	0.7253	5.1051	1.2739
7	4368	4468	2.2633	43.5814	0.1138	0.7445	2.4629	18.6119	4.2903

Table 23: *Ex. 4.* Time for assembling and solving of systems generating d.o.f. of  $u_h$  and  $\mathbf{y}_h$  as well as the time spent on e/w evaluation of error, majorant, and residual error estimator w.r.t. adaptive ref. steps,  $\mathbf{y}_h \in S_h^{3,3} \oplus S_h^{3,3}$ .

**Example 5** The final example with two-dimensional domain is defined on a quarter-annulus with the following exact solution and RHS:

$$\begin{aligned} u &= \cos x_1 e^{x^2} && \text{in } \Omega, \\ f &= 0 && \text{in } \Omega, \\ u_D &= \cos x_1 e^{x^2} && \text{on } \Gamma. \end{aligned}$$

Due to the IgA framework, the Dirichlet BC for the approximation  $u_h$  are fully satisfied, therefore, functional error estimates can be applied for the domains with curved boundaries providing a fully reliable (non-heuristic) error control. The results obtained for the adaptive refinement for  $u_h \in S_h^{2,2}$ ,  $\mathbf{y} \in S_{4h}^{4,4} \oplus S_{4h}^{4,4}$ , and bulk parameter  $\theta = 0.4$ , are illustrated in Tables 24–25. Again, even for such specific geometry, the generation of the optimal  $\mathbf{y}_h$  (assembling and solving the (28)) requires several times less computational effort than  $u_h$ :  $\frac{t_{\text{as}}(u_h)}{t_{\text{as}}(\mathbf{y}_h)} \approx \frac{38.5360}{19.1958} \approx 2$  and  $\frac{t_{\text{sol}}(u_h)}{t_{\text{sol}}(\mathbf{y}_h)} \approx \frac{3.4323}{0.4727} \approx 7$ . Moreover, in Figure 16, we illustrate the evolution of the meshes  $\hat{\mathcal{K}}_h$  and  $\mathcal{K}_h$  on the parametric  $\hat{\Omega}$  and physical  $\Omega$  domains, respectively.

**Example 6** Last two examples are dedicated to three-dimensional problems. Let  $\Omega = (0, 1)^3 \subset \mathbb{R}^3$ ,

$$\begin{aligned} u &= (1 - x_1) x_1^2 (1 - x_2) x_2^2 (1 - x_3) x_3^2 && \text{in } \Omega, \\ u_D &= 0 && \text{on } \Gamma. \end{aligned}$$

The uniform refinement strategy, assuming that  $u_h \in S_h^{2,2}$  and  $\mathbf{y}_h \in S_{6h}^{3,3} \oplus S_{6h}^{3,3}$ , provides numerical results illustrated in Tables 26 and 27. Comparison of the majorant performance to the accuracy of residual error

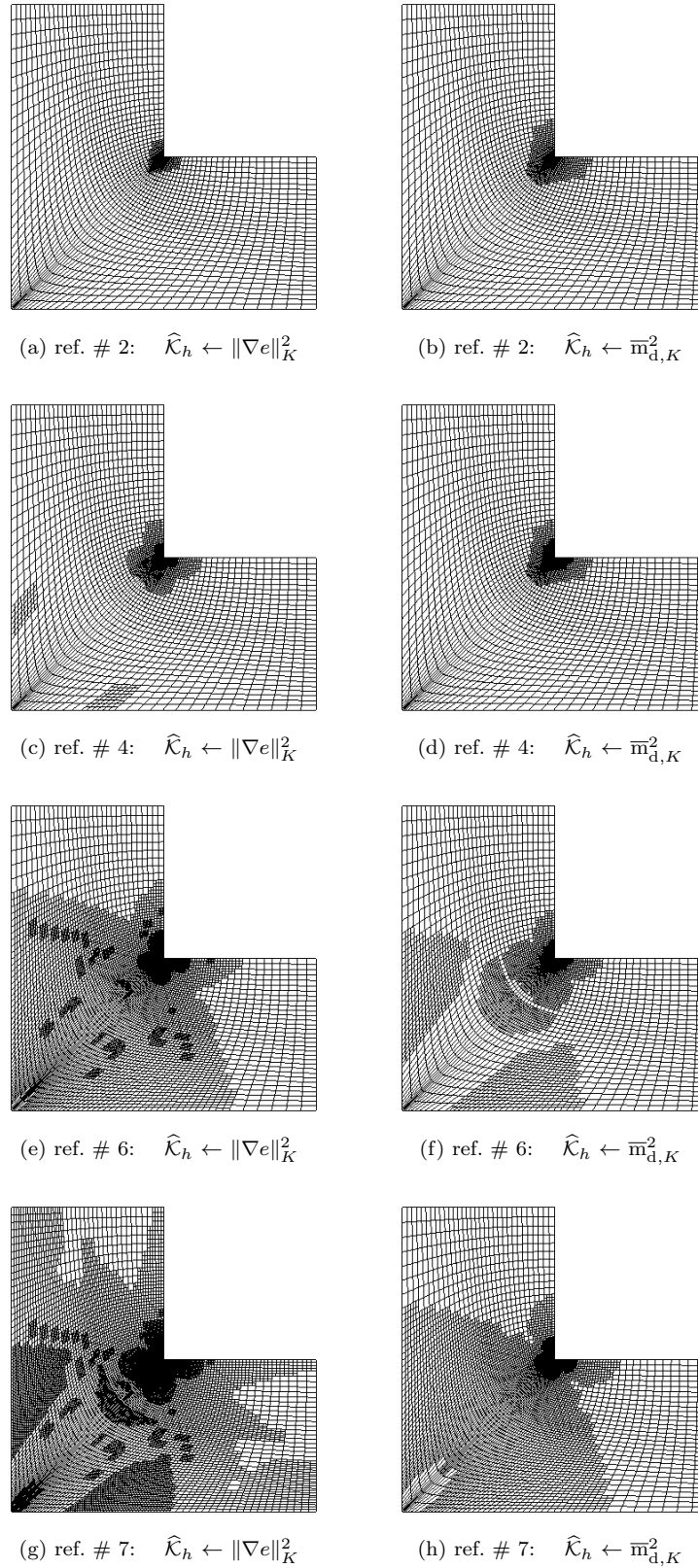
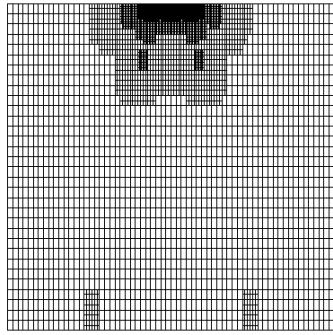
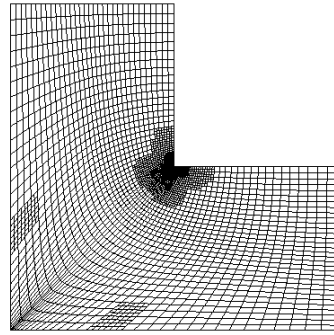


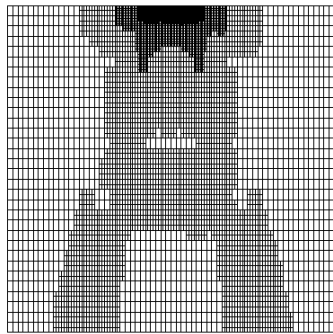
Figure 12: Comparison of the meshes generated by two refinement strategies, i.e., the true error (left) and error indicator provided by the majorant (right), with the marking criterion  $\mathbf{M}_{\text{BULK}}(0.2)$ .



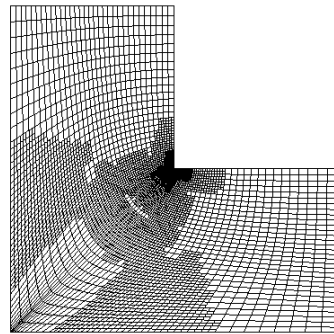
(a) ref. # 4:  $\widehat{\Omega}$  and  $\widehat{\mathcal{K}}_h$



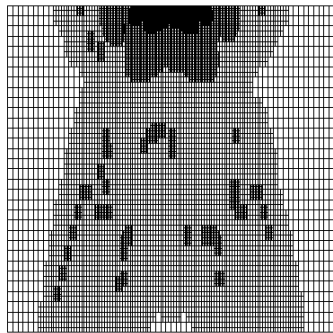
(b) ref. # 4:  $\Omega$  and  $\mathcal{K}_h$



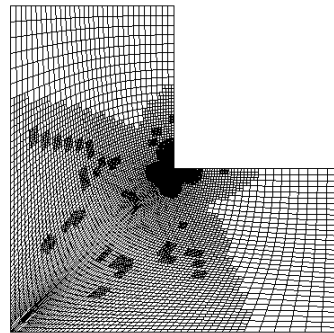
(c) ref. # 5:  $\widehat{\Omega}$  and  $\widehat{\mathcal{K}}_h$



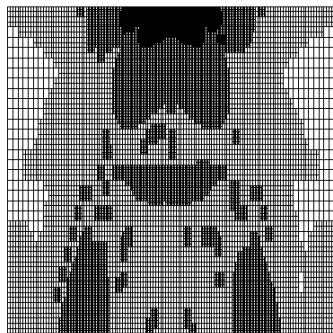
(d) ref. # 5:  $\Omega$  and  $\mathcal{K}_h$



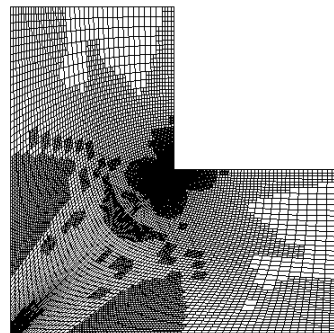
(e) ref. # 6:  $\widehat{\Omega}$  and  $\widehat{\mathcal{K}}_h$



(f) ref. # 6:  $\Omega$  and  $\mathcal{K}_h$



(g) ref. # 7:  $\widehat{\Omega}$  and  $\widehat{\mathcal{K}}_h$



(h) ref. # 7:  $\Omega$  and  $\mathcal{K}_h$

Figure 13: *Ex. 4.* Comparison of meshes on the physical and parametrical domains w.r.t. adaptive ref. steps,  $\mathbf{M}_{\text{BULK}}(0.1)$ .

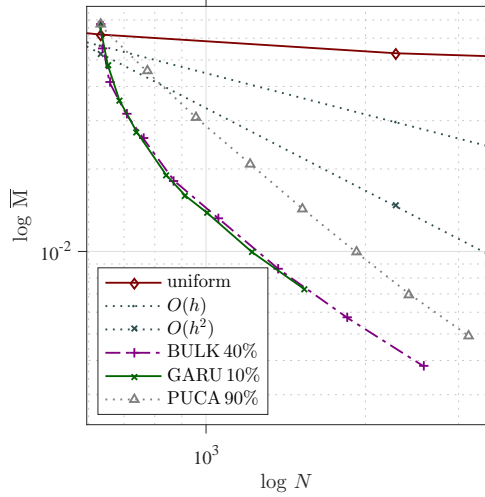


Figure 14: Convergence of majorant.

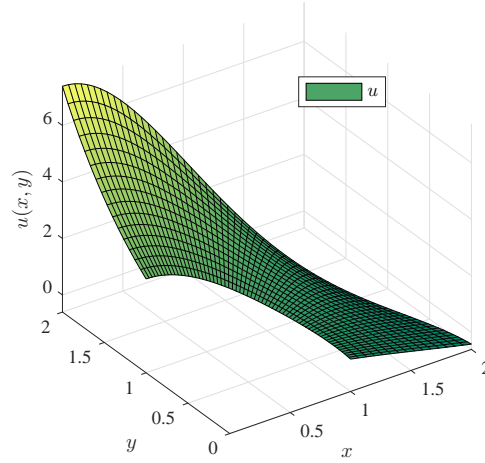


Figure 15: *Ex. 5.* Exact solution  $\cos(x_1) e^{x^2}$ .

# ref.	$\ \nabla e\ _{\Omega}$	$\bar{M}$	$\bar{m}_d^2$	$\bar{m}_{eq}^2$	$I_{\text{eff}}(\bar{M})$	$I_{\text{eff}}(\bar{\eta})$	e.o.c.
3	1.9377e-03	2.2682e-03	2.1466e-03	2.7011e-04	1.1706	8.0838	1.8290
5	2.7731e-04	3.9296e-04	3.7669e-04	3.6143e-05	1.4171	8.2886	2.1330
7	4.7689e-05	6.6456e-05	5.5448e-05	2.4453e-05	1.3935	8.3850	2.1653

Table 24: *Ex. 5.* Error, majorant (with dual and reliability terms), efficiency indices, error, e.o.c. w.r.t. adaptive ref. steps.

# ref.	# d.o.f. ( $u_h$ )	# d.o.f. ( $\mathbf{y}_h$ )	$t_{\text{as}}(u_h)$	$t_{\text{as}}(\mathbf{y}_h)$	$t_{\text{sol}}(u_h)$	$t_{\text{sol}}(\mathbf{y}_h)$	$t_{e/w}(\ \nabla e\ )$	$t_{e/w}(\bar{M})$	$t_{e/w}(\bar{\eta})$
1	324	400	0.1059	1.7198	0.0010	0.0245	0.1592	0.7331	0.3351
3	1389	400	0.4475	1.0655	0.0081	0.0166	0.5914	0.9428	1.1633
5	9125	400	5.0846	1.1225	0.1925	0.0363	5.1422	9.5749	9.1553
7	50291	1623	38.5360	19.1958	3.4323	0.4727	21.0657	96.3344	41.5038

Table 25: *Ex. 5.* Time for assembling and solving the systems generating d.o.f. of  $u_h$  and  $\mathbf{y}_h$  as well as the time spent on e/w evaluation of error, majorant, and residual error estimator w.r.t. adaptive ref. steps.

estimates, i.e.,  $I_{\text{eff}}(\bar{M}) = 1.2378$  and  $I_{\text{eff}}(\bar{\eta}) = 13.4166$ , confirms that the latter one always overestimates the error (even for such a smooth exact solution). Moreover, the computational costs of majorant generation is a hundred times less than the computational time for a primal variable, namely,  $\frac{t_{\text{as}}(u_h)}{t_{\text{as}}(\mathbf{y}_h)} \approx 578$ , and  $\frac{t_{\text{sol}}(u_h)}{t_{\text{sol}}(\mathbf{y}_h)} \approx 136$ . It is important to note that values of the last three columns of Table 27 illustrate sub-optimal time for the element-wise evaluation. As mentioned earlier, this issue is related to the implementation of element-wise iterator

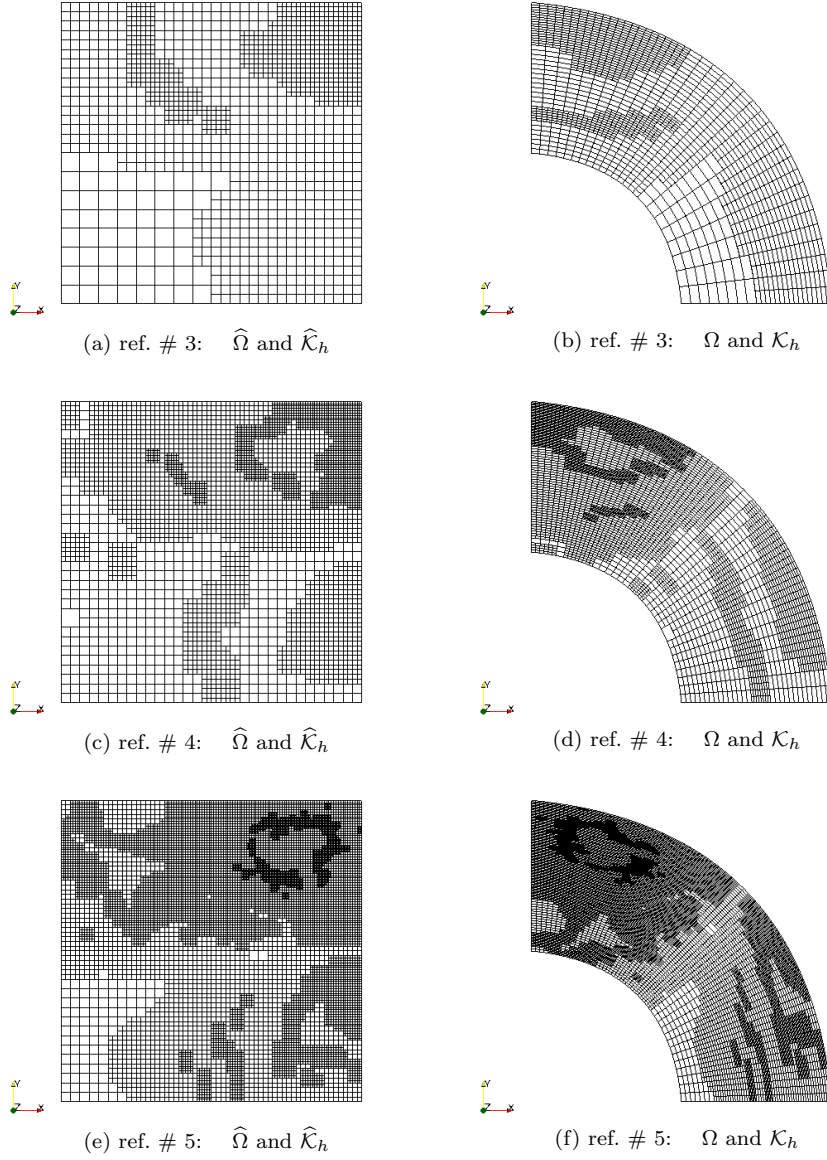


Figure 16: *Ex. 5.* Comparison of meshes on the physical and parametrical domains w.r.t. adaptive ref. steps.

# ref.	$\ \nabla e\ _{\Omega}$	$\bar{M}$	$\bar{m}_d^2$	$\bar{m}_{eq}^2$	$I_{\text{eff}}(\bar{M})$	$I_{\text{eff}}(\bar{\eta})$	e.o.c.
2	9.7268e-04	1.1328e-03	1.0104e-03	6.6641e-04	1.1646	14.2071	4.9421
4	5.7843e-05	7.9238e-05	7.8966e-05	1.4807e-06	1.3699	13.4654	2.7348
6	3.6029e-06	4.6376e-06	4.5126e-06	6.8010e-07	1.2872	13.4195	2.1808
8	2.2513e-07	2.8772e-07	2.7822e-07	5.1726e-08	1.2780	13.4166	2.0451

Table 26: *Ex. 6.* Error, majorant (with dual and reliability terms), efficiency indices, error, e.o.c. w.r.t. unif. ref. steps.

# ref.	# d.o.f. ( $u_h$ )	# d.o.f. ( $\mathbf{y}_h$ )	$t_{\text{as}}(u_h)$	$t_{\text{as}}(\mathbf{y}_h)$	$t_{\text{sol}}(u_h)$	$t_{\text{sol}}(\mathbf{y}_h)$	$t_{e/w}(\ \nabla e\ )$	$t_{e/w}(\bar{M})$	$t_{e/w}(\bar{\eta})$
2	64	64	0.0121	0.0292	0.0000	0.0131	0.0013	0.0079	0.0065
4	1000	64	0.1535	0.0477	0.0005	0.0084	0.1913	0.2480	0.2962
6	39304	64	6.2179	0.0529	0.2208	0.0106	11.7921	15.9026	17.5110
8	2197000	343	324.7514	0.5641	54.6425	0.1760	560.9245	452.5727	865.4832

Table 27: *Ex. 6.* Time for assembling and solving the systems generating d.o.f. of  $u_h$  and  $\mathbf{y}_h$  as well as the time spent on e/w evaluation of error, majorant, and residual error estimator w.r.t. unif. ref. steps.

currently used in G+Smo and will be addressed in the follow-up reports. The results obtained while performing

# ref.	$\ \nabla e\ _\Omega$	$\bar{M}$	$\bar{m}_d^2$	$\bar{m}_{eq}^2$	$I_{\text{eff}}(\bar{M})$	$I_{\text{eff}}(\bar{\eta})$	e.o.c.
3	2.3387e-04	2.7678e-04	2.7288e-04	2.1210e-05	1.1835	13.6135	3.5152
5	1.9918e-05	2.7263e-05	2.3917e-05	1.8207e-05	1.3687	11.7620	2.2298
7	2.2272e-06	3.1275e-06	2.9019e-06	1.2276e-06	1.4042	12.4614	2.0710

Table 28: *Ex. 6.* Error, majorant (with dual and reliability terms), efficiency indices, error, e.o.c. w.r.t. adaptive ref. steps.

# ref.	# d.o.f.( $u_h$ )	# d.o.f.( $\mathbf{y}_h$ )	$t_{\text{as}}(u_h)$	$t_{\text{as}}(\mathbf{y}_h)$	$t_{\text{sol}}(u_h)$	$t_{\text{sol}}(\mathbf{y}_h)$	$t_{e/w}(\ \nabla e\ )$	$t_{e/w}(\bar{M})$	$t_{e/w}(\bar{\eta})$
1	27	64	0.0146	0.0718	0.0000	0.0049	0.0066	0.0445	0.0213
3	216	64	0.3379	0.0773	0.0001	0.0107	0.4165	0.8699	1.0376
5	4074	64	21.5658	0.0837	0.0420	0.0074	26.7396	39.1294	50.8124
7	127265	64	3054.9337	0.0838	3.2532	0.0087	1415.2231	1720.7416	2433.3058

Table 29: *Ex. 6.* Time for assembling and solving the systems generating d.o.f. of  $u_h$  and  $\mathbf{y}_h$  as well as the time spent on e/w evaluation of error, majorant, and residual error estimator w.r.t. adaptive ref. steps.

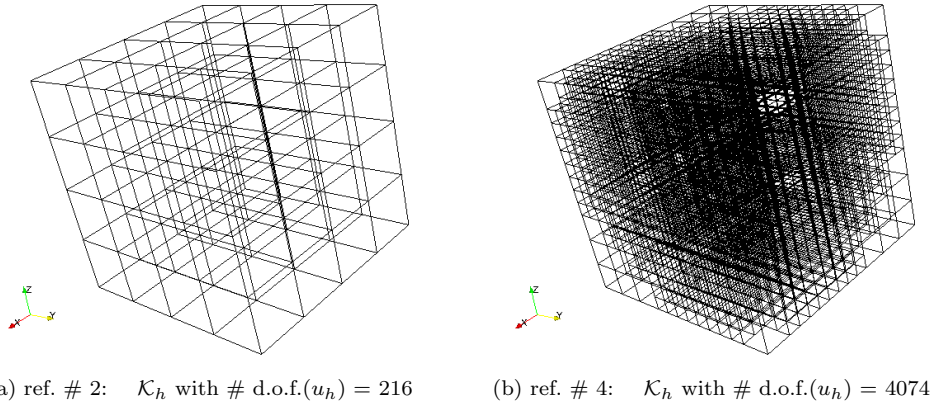


Figure 17: *Ex. 6.* Evolution of meshes on the physical unit cube w.r.t. adaptive ref. steps with bulk marking criterion  $\mathbf{M}_{\text{BULK}}(0.4)$ .

an adaptive refinement strategy with the bulk marking criterion  $\mathbf{M}_{\text{BULK}}(0.4)$  are summarised in Tables 28–29. The obtained ratios between majorants and the true error as well as the computational time it requires to be generated, i.e.,

$$\frac{t_{\text{as}}(u_h)}{t_{\text{as}}(\mathbf{y}_h)} \approx \frac{324.75145}{0.5641} \approx 575 \quad \text{and} \quad \frac{t_{\text{sol}}(u_h)}{t_{\text{sol}}(\mathbf{y}_h)} \approx \frac{54.6425}{0.1760} \approx 310,$$

confirm the efficiency of the functional approach to the error control for these type of problems. The mesh evolution for the considered adaptive refinement strategy is illustrated in Figure 17 (just for two refinement steps). One can see that the main refinement is performed closer to the centre of the computational domain  $\Omega$ , which is similar to the results obtained for two-dimensional case.

**Example 7** Finally, in the last example, we test functional error estimates on a complex three-dimensional geometry of a  $G$ -shape. The exact solution, RHS, and Dirichlet BC are defined as follows:

$$\begin{aligned} u &= 10 \cos x_1 e^{x_2} x_3 && \text{in } \Omega, \\ f &= 0 && \text{in } \Omega, \\ u_D &= 10 \cos x_1 e^{x_2} x_3 && \text{on } \Gamma. \end{aligned}$$

Let us consider  $N_{\text{ref},0} = 1$  initial unif. ref. step of the mesh assigned to the geometry (illustrated in Figure 18). The numerical results of 5 adaptive ref. steps are summarised in Tables 30–31. From Table 30 analysing the efficiency of the error estimates, it is obvious that  $\bar{M}$  is at least 40 times sharper than the residual error indicator. If one analyses the computation costs, it is easy to notice that the assembling time of the system (28) is better than the assembling time of (26), i.e.,  $\frac{t_{\text{as}}(u_h)}{t_{\text{as}}(\mathbf{y}_h)} \approx 14$ . However, the costs for solving the system (28) is higher, i.e.,  $\frac{t_{\text{sol}}(u_h)}{t_{\text{sol}}(\mathbf{y}_h)} \approx \frac{1}{12}$ . The element-wise evaluation of  $\|\nabla e\|$ ,  $\bar{M}$ , and  $\bar{\eta}$  must take at least as long as  $t_{\text{as}}(u_h)$  (since both are performed with  $u_h$  element-wise), which is confirmed in the last three columns of Table 31.

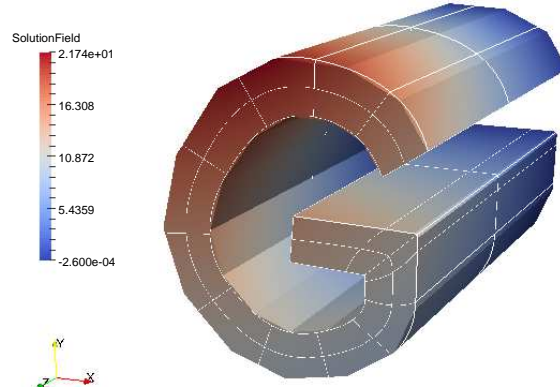


Figure 18: *Ex. 7.* Exact solution  $u = 10 \cos x_1 e^{x_2} x_3$ .

# ref.	$\ \nabla e\ _{\Omega}$	$\bar{M}$	$\bar{m}_d^2$	$\bar{m}_{eq}^2$	$I_{\text{eff}}(\bar{M})$	$I_{\text{eff}}(\bar{\eta})$	e.o.c.
3	1.5495e-02	1.6552e-02	1.6016e-02	2.9195e-03	1.0682	42.1400	3.1601
4	5.5530e-03	6.7468e-03	6.0466e-03	3.8103e-03	1.2150	59.4362	3.0093
5	2.3080e-03	3.6335e-03	2.7857e-03	4.6130e-03	1.5743	47.1796	2.5110

Table 30: *Ex. 7.* Error, majorant (with dual and reliability terms), efficiency indices, error, e.o.c. w.r.t. adaptive ref. steps.

# ref.	# d.o.f. ( $u_h$ )	# d.o.f. ( $\mathbf{y}_h$ )	$t_{\text{as}}(u_h)$	$t_{\text{as}}(\mathbf{y}_h)$	$t_{\text{sol}}(u_h)$	$t_{\text{sol}}(\mathbf{y}_h)$	$t_{e/w}(\ \nabla e\ )$	$t_{e/w}(\bar{M})$	$t_{e/w}(\bar{\eta})$
3	1108	575	8.5398	3.4636	0.0056	3.2101	11.8510	7.5239	21.5933
4	3082	575	31.4262	2.9348	0.0686	3.7503	38.9502	26.7215	77.4521
5	8798	575	97.6563	7.1416	0.2659	3.1107	122.7187	101.5395	229.4474

Table 31: *Ex. 7.* Time for assembling and solving the systems generating d.o.f. of  $u_h$  and  $\mathbf{y}_h$  as well as the time spent on e/w evaluation of error, majorant, and residual error estimator w.r.t. adaptive ref. steps.

The evolution of the meshes on both physical and parametric domains is illustrated in Figure 19. The final solution and meshes obtained in the final step are presented in Figure 20. The latter plots are presented from the axis  $O_z$  view-point so that the reader can clearly see the finer parts of the physical and parametric meshes.

## Conclusion

In the paper, we have numerically studied two-sided functional error estimates in the framework of IgA schemes. The very first derivation of these type of error bounds dates back to 96'-97' (see [59, 60]). The generalised functional approach applied in these works allows obtaining estimates of the error between exact solution and any approximation from the admissible energy space (independently on the numerical method used for the reconstruction of this approximation). As the consequence, discussed estimates do not depend on any mesh dependent constants and do not pose any requirements (such as Galerkin's orthogonality) on the approximate solution. The pioneering study, investigating the application of the majorant to IgA approximations generated by tensor-product splines in a context of elliptic BVP, can be found in [28]. Current work extends the study of the fully reliable adaptive IgA schemes using THB-splines in combination with the functional two-sided bounds and the local error indicators generated by them.

In this study, we have highlighted main numerical properties of the functional error estimates in the context of both reliable global energy error estimation and efficient local error distribution indication. We mainly focused on the algorithmic and implementational parts of two-sided bounds application as well as details of their integration into the IgA framework. Presented examples and corresponding numerical results have provided an convincing evidence of the global reliability of the majorant and even more importantly local efficiency of the error indicator generated by it. Implementation of all the methods was carried out using open source C++ library G+Smo developed primarily by research groups of RICAM and JKU, Linz [38].

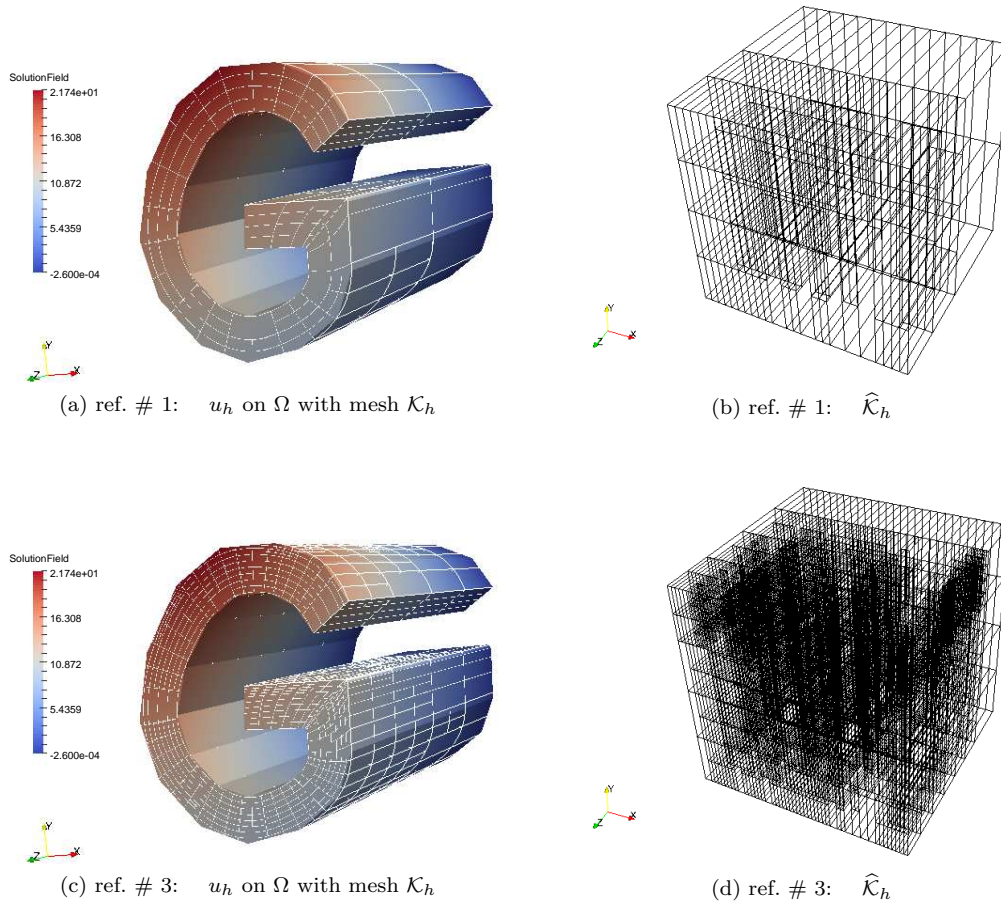


Figure 19: *Ex. 7.* Comparison of meshes on the physical and parametrical domains w.r.t. adaptive ref. steps.

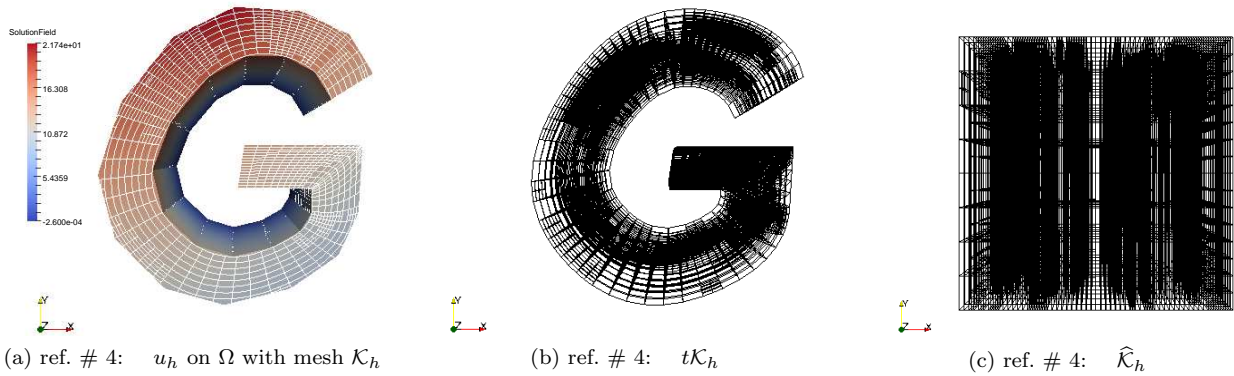


Figure 20: *Ex. 7.* Solution on the domain  $\Omega$  and corresponding meshes on physical and parametrical domains, view from the axis  $0_z$ .

In the majority of the numerical tests presented by Section 5, we were able to take an advantage of the smoothness of B-(THB-)splines and to reconstruct auxiliary functions used by majorant and minorant exploiting higher order splines and coarser meshes (in comparison to the primal approximation) in order to achieve the considerable speed-up in the time required for reliable error estimation. It naturally allowed to decrease the overall computational time considerably. However, for some problems with highly oscillating solutions or solutions possessing singularities, coarsening of the mesh used for the auxiliary functions decreases the quality of their reconstruction and, as the consequence lowers the effectiveness of the majorant and minorant. Therefore,

we had to invest more time to reconstruct sufficiently accurate  $\mathbf{y}_h$  and  $w_h$  reconstructions. This computational time overhead for assembling and solving systems generated from the minimisation of  $\bar{M}$  (maximisation of  $\underline{M}$ ) can be however minimised by multi-core parallelisation, which stayed out of the focus of the current paper.

Throughout Section 5, majorant has been compared to the residual-type error estimate, i.e., its performance confirmed to be always more stable and efficient in comparison to  $\bar{\eta}$ . Indeed, it requires more time for optimising majorant but also reassures that the error is controlled in a reliable way and its local distribution is indicated correctly. Both upper and lower bounds were tested w.r.t. to different marking criterions to make sure that they provide an efficient local indication of the error. Meshes produced by the refinement based on the indicator that follows from  $\bar{M}$  were compared to the meshes obtained by the adaptive strategy using the true error distribution. The topology of these meshes appeared to be very close, which confirmed the effectiveness of the majorant application in designing a fully adaptive numerical scheme. If the exact solution is not provided, the quality of the majorant can be verified by comparison of its values to the minorant of the error. That was demonstrated in several numerical examples, where the ration between  $\bar{M}$  and  $\underline{M}$  remained close to one.

The universality of the functional error estimates allows to easily extend them to parabolic problems. The corresponding results on the application of these error bounds to space-time IgA techniques in a context of evolutionary problems can be found in [34].

**Acknowledgments** The research is supported by the Austrian Science Fund (FWF) through the NFN S117-03 project. Implementation was carried out using the open-source C++ library G+Smo [38].

## References

- [1] Y. Bazilevs, V. M. Calo, J. A. Cottrell, J. A. Evans, T. J. R. Hughes, S. Lipton, M. A. Scott, and T. W. Sederberg. Isogeometric analysis using T-splines. *Comput. Methods Appl. Mech. Engrg.*, 199(5-8):229–263, 2010.
- [2] M. Bebendorf. A note on the Poincaré inequality for convex domains. *Z. Anal. Anwendungen*, 22(4):751–756, 2003.
- [3] L. Beirão da Veiga, A. Buffa, D. Cho, and G. Sangalli. Analysis-suitable T-splines are dual-compatible. *Comput. Methods Appl. Mech. Engrg.*, 249/252:42–51, 2012.
- [4] L. Beirão da Veiga, A. Buffa, D. Cho, and G. Sangalli. IsoGeometric analysis using T-splines on two-patch geometries. *Comput. Methods Appl. Mech. Engrg.*, 200(21-22):1787–1803, 2011.
- [5] F. A. Bornemann and P. Deuffhard. The cascadic multigrid method for elliptic problems. *Numer. Math.*, 75(2):135–152, 1996.
- [6] A. Bressan. Some properties of LR-splines. *Comput. Aided Geom. Design*, 30(8):778–794, 2013.
- [7] A. Bressan and B. Jüttler. A hierarchical construction of LR meshes in 2D. *Comput. Aided Geom. Design*, 37:9–24, 2015.
- [8] A. Buffa and C. Giannelli. Adaptive isogeometric methods with hierarchical splines: error estimator and convergence. Technical Report arxiv: 1502.00565, arxiv:math.NA, 2015.
- [9] L. Beirão Da Veiga, A. Buffa, G. Sangalli, and R. Vázquez. Analysis-suitable T-splines of arbitrary degree: definition, linear independence and approximation properties. *Math. Models Methods Appl. Sci.*, 23(11):1979–2003, 2013.
- [10] L. Dedè and H. A. F. A. Santos. B-spline goal-oriented error estimators for geometrically nonlinear rods. *Comput. Mech.*, 49(1):35–52, 2012.
- [11] J. Deng, F. Chen, X. Li, C. Hu, W. Tong, Z. Yang, and Y. Feng. Polynomial splines over hierarchical t-meshes. *Graph. Models*, 70:76–86, 2008.
- [12] P. Deuffhard. Cascadic conjugate gradient methods for elliptic partial differential equations: algorithm and numerical results. In *Domain decomposition methods in scientific and engineering computing (University Park, PA, 1993)*, volume 180 of *Contemp. Math.*, pages 29–42. Amer. Math. Soc., Providence, RI, 1994.
- [13] T. Dokken, T. Lyche, and K. F. Pettersen. Polynomial splines over locally refined box-partitions. *Comput. Aided Geom. Design*, 30(3):331–356, 2013.
- [14] M. R. Dörfel, B. Jüttler, and B. Simeon. Adaptive isogeometric analysis by local  $h$ -refinement with T-splines. *Comput. Methods Appl. Mech. Engrg.*, 199(5-8):264–275, 2010.
- [15] W. Dörfler. A convergent adaptive algorithm for Poisson’s equation. *SIAM J. Numer. Anal.*, 33(3):1106–1124, 1996.
- [16] E. J. Evans, M. A. Scott, X. Li, and D. C. Thomas. Hierarchical T-splines: analysis-suitability, Bézier extraction, and application as an adaptive basis for isogeometric analysis. *Comput. Methods Appl. Mech. Engrg.*, 284:1–20, 2015.
- [17] D.R. Forsey and R.H. Bartels. Hierarchical b-spline refinement. *Comput. Graphics*, 22:205–212, 1988.

- [18] K. Friedrichs. On certain inequalities and characteristic value problems for analytic functions and for functions of two variables. *Trans. Amer. Math. Soc.*, 41(3):321–364, 1937.
- [19] C. Giannelli and B. Jüttler. Bases and dimensions of bivariate hierarchical tensor-product splines. *J. Comput. Appl. Math.*, 239:162–178, 2013.
- [20] C. Giannelli, B. Jüttler, S. K. Kleiss, A. Mantzaflaris, B. Simeon, and J. Speh. THB-splines: an effective mathematical technology for adaptive refinement in geometric design and isogeometric analysis. *Comput. Methods Appl. Mech. Engrg.*, 299:337–365, 2016.
- [21] C. Giannelli, B. Jüttler, and H. Speleers. THB-splines: the truncated basis for hierarchical splines. *Comput. Aided Geom. Design*, 29(7):485–498, 2012.
- [22] C. Giannelli, B. Jüttler, and H. Speleers. Strongly stable bases for adaptively refined multilevel spline spaces. *Adv. Comput. Math.*, 40(2):459–490, 2014.
- [23] G. Greiner and K. Hormann. Interpolating and approximating scattered 3D data with hierarchical tensor product  $B$ -splines. In *Surface fitting and multiresolution methods (Chamonix-Mont-Blanc, 1996)*, pages 163–172. Vanderbilt Univ. Press, Nashville, TN, 1997.
- [24] T. J. R. Hughes, J. A. Cottrell, and Y. Bazilevs. Isogeometric analysis: CAD, finite elements, NURBS, exact geometry and mesh refinement. *Comput. Methods Appl. Mech. Engrg.*, 194(39-41):4135–4195, 2005.
- [25] T. J. R. Hughes, J. A. Cottrell, and Y. Bazilevs. *Isogeometric Analysis: Toward Integration of CAD and FEA*. John Wiley & Sons, 2009.
- [26] K. A. Johannessen, F. Remonato, and T. Kvamsdal. On the similarities and differences between classical hierarchical, truncated hierarchical and LR B-splines. *Comput. Methods Appl. Mech. Engrg.*, 291:64–101, 2015.
- [27] K.A. Johannessen. *An adaptive isogeometric finite element analysis*. PhD thesis, Master’s thesis, Norwegian University of Science and Technology, 2009.
- [28] S. K. Kleiss and S. K. Tomar. Guaranteed and sharp a posteriori error estimates in isogeometric analysis. *Comput. Math. Appl.*, 70(3):167–190, 2015.
- [29] R. Kraft. Adaptive and linearly independent multilevel  $B$ -splines. In *Surface fitting and multiresolution methods (Chamonix-Mont-Blanc, 1996)*, pages 209–218. Vanderbilt Univ. Press, Nashville, TN, 1997.
- [30] M. Kumar, T. Kvamsdal, and K. A. Johannessen. Simple a posteriori error estimators in adaptive isogeometric analysis. *Comput. Math. Appl.*, 70(7):1555–1582, 2015.
- [31] G. Kuru. *Goal-Adaptive Isogeometric Analysis with Hierarchical Splines*. PhD thesis, Master’s thesis, Mechanical Engineering, Eindhoven University of Technology, 2013.
- [32] G. Kuru, C. V. Verhoosel, K. G. van der Zee, and E. H. van Brummelen. Goal-adaptive isogeometric analysis with hierarchical splines. *Comput. Methods Appl. Mech. Engrg.*, 270:270–292, 2014.
- [33] O. A. Ladyzhenskaya. *The boundary value problems of mathematical physics*. Springer, New York, 1985.
- [34] U. Langer, S. Matculevich, and S. Repin. Guaranteed error control bounds for the stabilised space-time iga approximations to parabolic problems. Technical Report arXiv:1712.06017v2, arxiv:math.NA, 2018.
- [35] R. Lazarov, S. Repin, and S. K. Tomar. Functional a posteriori error estimates for discontinuous Galerkin approximations of elliptic problems. *Numer. Methods Partial Differential Equations*, 25(4):952–971, 2009.
- [36] X. Li, J. Zheng, T. W. Sederberg, Th. J. R. Hughes, and M. A. Scott. On linear independence of T-spline blending functions. *Comput. Aided Geom. Design*, 29(1):63–76, 2012.
- [37] O. Mali, P. Neittaanmäki, and S. Repin. *Accuracy verification methods*, volume 32 of *Computational Methods in Applied Sciences*. Springer, Dordrecht, 2014. Theory and algorithms.
- [38] A. et all Mantzaflaris. G+smo (geometry plus simulation modules) v0.8.1. <http://gs.jku.at/gismo>, 2015.
- [39] S. Matculevich, P. Neittaanmäki, and S. Repin. A posteriori error estimates for time-dependent reaction-diffusion problems based on the Payne–Weinberger inequality. *AIMS*, 35(6):2659–2677, 2015.
- [40] S. Matculevich and S. Repin. Computable bounds of the distance to the exact solution of parabolic problems based on Poincaré type inequalities. *Zap. Nauchn. Sem. S.-Peterburg. Otdel. Mat. Inst. Steklov (POMI)*, 425(1):7–34, 2014.
- [41] S. Matculevich and S. Repin. Estimates for the difference between exact and approximate solutions of parabolic equations on the basis of Poincaré inequalities for traces of functions on the boundary. *Differential Equations*, 52(10):1355–1365, 2016.
- [42] S. Matculevich and S. Repin. Explicit constants in Poincaré-type inequalities for simplicial domains. *Computational Methods in Applied Mathematics - CMAM*, 16(2):277–298, 2016.
- [43] P. Morgenstern and D. Peterseim. Analysis-suitable adaptive T-mesh refinement with linear complexity. *Comput. Aided Geom. Design*, 34:50–66, 2015.

- [44] A. I. Nazarov and S. I. Repin. Exact constants in Poincaré type inequalities for functions with zero mean boundary traces. *Mathematical Methods in the Applied Sciences*, 2014. Published in arXiv.org in 2012, math/1211.2224.
- [45] P. Neittaanmäki and S. Repin. *Reliable methods for computer simulation*, volume 33 of *Studies in Mathematics and its Applications*. Elsevier Science B.V., Amsterdam, 2004. Error control and a posteriori estimates.
- [46] N. Nguyen-Thanh, H. Nguyen-Xuan, S. P. A. Bordas, and T. Rabczuk. Isogeometric analysis using polynomial splines over hierarchical T-meshes for two-dimensional elastic solids. *Comput. Methods Appl. Mech. Engrg.*, 200(21-22):1892–1908, 2011.
- [47] N. Nguyen-Thanh and K. Zhou. Extended isogeometric analysis based on PHT-splines for crack propagation near inclusions. *International Journal for Numerical Methods in Engineering*, 112:1777–1800, 2017.
- [48] L. E. Payne and H. F. Weinberger. An optimal Poincaré inequality for convex domains. *Arch. Rational Mech. Anal.*, 5:286–292 (1960), 1960.
- [49] L. Piegl and W. Tiller. *The NURBS book*. Springer Berlin Heidelberg, 1997.
- [50] H. Poincaré. Sur les Equations aux Derivees Partielles de la Physique Mathematique. *Amer. J. Math.*, 12(3):211–294, 1890.
- [51] H. Poincaré. Sur les Equations de la Physique Mathematique. *Rend. Circ. Mat. Palermo*, 8:57–156, 1894.
- [52] S. Repin. *A posteriori estimates for partial differential equations*, volume 4 of *Radon Series on Computational and Applied Mathematics*. Walter de Gruyter GmbH & Co. KG, Berlin, 2008.
- [53] S. Repin. *A posteriori estimates for partial differential equations*, volume 4 of *Radon Series on Computational and Applied Mathematics*. Walter de Gruyter GmbH & Co. KG, Berlin, 2008.
- [54] S. Repin. Estimates of constants in boundary-mean trace inequalities and applications to error analysis. In *Numerical Mathematics and Advanced Applications - ENUMATH 2013*, volume 103 of *Lecture Notes in Computational Science and Engineering*, pages 215–223. Springer, Switzerland, 2015.
- [55] S. Repin, S. Sauter, and A. Smolianski. A posteriori error estimation for the Dirichlet problem with account of the error in the approximation of boundary conditions. *Computing*, 70(3):205–233, 2003.
- [56] S. Repin, S. Sauter, and A. Smolianski. A posteriori error estimation for the Poisson equation with mixed Dirichlet/Neumann boundary conditions. In *Proceedings of the 10th International Congress on Computational and Applied Mathematics (ICCAM-2002)*, volume 164/165, pages 601–612, 2004.
- [57] S. Repin, S. Sauter, and A. Smolianski. Two-sided a posteriori error estimates for mixed formulations of elliptic problems. *SIAM J. Numer. Anal.*, 45(3):928–945, 2007.
- [58] S. Repin and A. Smolianski. Functional-type a posteriori error estimates for mixed finite element methods. *Russian J. Numer. Anal. Math. Modelling*, 20(4):365–382, 2005.
- [59] S. I. Repin. A posteriori error estimation for nonlinear variational problems by duality theory. *Zapiski Nauchnykh Seminarov POMI*s, 243:201–214, 1997.
- [60] S. I. Repin. A posteriori error estimates for approximate solutions to variational problems with strongly convex functionals. *Journal of Mathematical Sciences*, 97:4311–4328, 1999.
- [61] Sergey I. Repin and Satyendra K. Tomar. Guaranteed and robust error bounds for nonconforming approximations of elliptic problems. *IMA J. Numer. Anal.*, 31(2):597–615, 2011.
- [62] D. Schillinger, L. Dedé, M.A. Scott, J.A. Evans, M.J. Borden, E. Rank, and T.J.R. Hughes. An isogeometric design-through-analysis methodology based on adaptive hierarchical refinement of NURBS, immersed boundary methods, and T-spline CAD surfaces. *Comput. Methods Appl. Mech. Engrg.*, 249/252:116–150, 2012.
- [63] M. A. Scott, M. J. Borden, C. V. Verhoosel, T. W. Sederberg, and T. J. R. Hughes. Isogeometric finite element data structures based on Bézier extraction of T-splines. *Internat. J. Numer. Methods Engrg.*, 88(2):126–156, 2011.
- [64] M. A. Scott, X. Li, T. W. Sederberg, and T. J. R. Hughes. Local refinement of analysis-suitable T-splines. *Comput. Methods Appl. Mech. Engrg.*, 213/216:206–222, 2012.
- [65] T. W. Sederberg, D. C. Cardon, G. T. Finnigan, N. N. North, J. Zheng, and T. Lyche. T-splines simplification and local refinement. *ACM Trans. Graphics*, 23(3):276–283, 2004.
- [66] T. W. Sederberg, J. Zheng, A. Bakenov, and A. Nasri. T-splines and t-nurccs. *ACM Trans. Graphics*, 22(3):477–484, 2003.
- [67] H. Speleers and C. Manni. Effortless quasi-interpolation in hierarchical spaces. *Numer. Math.*, 132(1):155–184, 2016.
- [68] S. K. Tomar and S. I. Repin. Efficient computable error bounds for discontinuous Galerkin approximations of elliptic problems. *J. Comput. Appl. Math.*, 226(2):358–369, 2009.
- [69] K. G. van der Zee and C. V. Verhoosel. Isogeometric analysis-based goal-oriented error estimation for free-boundary problems. *Finite Elem. Anal. Des.*, 47(6):600–609, 2011.

- [70] A.-V. Vuong, C. Giannelli, B. Jüttler, and B. Simeon. A hierarchical approach to adaptive local refinement in isogeometric analysis. *Comput. Methods Appl. Mech. Engrg.*, 200(49-52):3554–3567, 2011.
- [71] P. Wang, J. Xu, J. Deng, and F. Chen. Adaptive isogeometric analysis using rational pht-splines. *Computer-Aided Design*, 43(11):1438–1448, 2011.
- [72] X. Wei, Y. Zhang, T. J. R. Hughes, and M. A. Scott. Truncated hierarchical Catmull-Clark subdivision with local refinement. *Comput. Methods Appl. Mech. Engrg.*, 291:1–20, 2015.
- [73] J. Wloka. *Partial Differential Equations*. Cambridge University Press, 1987.
- [74] M. Wu, J. Xu, R. Wang, and Z. Yang. Hierarchical bases of spline spaces with highest order smoothness over hierarchical T-subdivisions. *Comput. Aided Geom. Design*, 29(7):499–509, 2012.
- [75] E. Zeidler. *Nonlinear functional analysis and its applications. II/A*. Springer-Verlag, New York, 1990.
- [76] U. Zore and B. Jüttler. Adaptively refined multilevel spline spaces from generating systems. *Comput. Aided Geom. Design*, 31(7-8):545–566, 2014.
- [77] U. Zore, B. Jüttler, and J. Kosinka. On the linear independence of truncated hierarchical generating systems. *J. Comput. Appl. Math.*, 306:200–216, 2016.